Economic Geology, v. 110, pp. 2041–2062

Textural Relationship of Sulfide Ores, PGE, and Sr-Nd-Os Isotope Compositions of the Triassic Piaohechuan Ni-Cu Sulfide Deposit in NE China

Bo Wei,[1] Christina Yan Wang,[1,†] Nicholas T. Arndt,[2] Hazel M. Prichard,[3] and Peter C. Fisher[3]

[1] *Key Laboratory of Mineralogy and Metallogeny, Guangzhou Institute of Geochemistry, Chinese Academy of Sciences, Guangzhou 510640, China*

[2] *LGCA, UMR 5025 CNRS, Université Joseph Fourier à Grenoble, BP53, 38041 Grenoble Cedex, France*

[3] *School of Earth and Ocean Sciences, Main Building, Park Place, Cardiff University, Cardiff, CF10 3AT, United Kingdom*

Abstract

The ~216-Ma Piaohechuan no. 4 intrusion in northeastern China, situated in the easternmost part of the Central Asian orogenic belt, is composed of hornblende-olivine gabbro overlain by hornblende gabbro. The intrusion is about 630 m long, 40 to 250 m wide, and 50 to 150 m thick. Nickel sulfide mineralization is restricted to the lower part of the intrusion and contains 10,000 metric tons (t) of Ni with average PGE concentrations of 40 ppb Os, 30 ppb Ir, 36 ppb Ru, 26 ppb Rh, 255 ppb Pt and 161 ppb Pd in 100% sulfide.

The sulfide ores display some distinctive textures and can be divided into "globular ores," which comprise millimeter- to centimeter-sized spherical to irregular patches of sulfide in a gabbroic matrix, "network ores" in which irregular sulfide aggregates with cuspate margins are intergrown at a scale of millimeters to centimeters with roughly equal proportion of gabbro, and "breccia ores" in which centimeter- to micron-sized fragments of gabbro or broken crystals from the gabbro are enclosed in a sulfide matrix. The silicate portions of the three types of sulfide ores are almost totally altered and only some fragments in the breccia ores are fresh. Pyrrhotite and pentlandite are the dominant sulfides in the ores and chalcopyrite is largely confined to finer fractures and patches in the silicate rocks. The Cu-rich ores are sparsely distributed in the orebody and are richer in Pt and Pd than other ores, consistent with fractionation of Cu and PGE during crystallization of sulfide liquid. Breccia and network ores have Pt ranging from 1.72 to 205 ppb, with positive and negative Pt anomalies in primitive mantle-normalized chalcophile element patterns. The high Pt concentrations of some ores are manifested by the sporadic occurrence of sperrylite.

Nickel in olivine decreases rapidly (2,258–393 ppm) with decreasing Fo (86–72). Small sulfide droplets are enclosed in olivine, indicating that olivine crystallized from sulfide-saturated magma. The rocks of the intrusion have restricted $\varepsilon_{Nd(t = 216\ Ma)}$ (4.4–4.6) and variable $\gamma_{Os(t = 216\ Ma)}$ values (39–67), consistent with the assimilation of external crustal sulfide in a shallow magma chamber. We propose that sulfide saturation was achieved by olivine fractionation and the addition of crustal sulfide. Early segregated sulfide liquid settled toward the base of the magma chamber and then migrated through partially molten silicates, along small channelways. The migrating sulfide liquid may have displaced and disaggregated the silicate melt or cumulus crystals into small fragments, creating the network and breccia ores. The globular ores formed when the coalesced sulfide droplets were largely solid before the final solidification of silicate minerals. Although the distance of migration is unconstrained, such migration of sulfide liquid had significant controls on the distribution of ores in the intrusion. At lower temperatures, metamorphism transformed part of the intrusion to low-grade hydrous assemblages and resulted in weak redistribution of sulfides and secondary silicate minerals.

Introduction

Ni-Cu sulfide deposits such as those at Norilsk-Talnakh in Russia, Kambalda in Western Australia, or Raglan in Canada form when an immiscible sulfide liquid segregates and accumulates in the lower part of a lava flow or sill (Lesher, 1983, 2007; Barnes et al., 1988; Naldrett et al., 1992; Arndt, 2011). The major control on the distribution of ore is the high density of sulfide liquid, which combined with its low viscosity allows it settle out from flowing magma (de Bremond d'Ars et al., 2001; Holzheid, 2010) or migrate downward through crystal mush (Stifter et al., 2014).

Distinct sulfide ore textures may contain important information for understanding the process of sulfide melt migration in magma conduit and the mobilization of sulfide during hydrothermal processes and metamorphism. Globular texture, large patches or globules of 100% sulfide disseminated at concentrations of a few percent in silicate rock, has been documented in many Ni sulfide deposits, for example, the Black Swan deposit in Western Australia (Dowling et al., 2004) and the Sudbury Complex (Naldrett, 1969), and in some dolerite dikes such as those described from a dike swarm in Uruguay (Prichard et al., 2004) and the Kangerlussuaq macrodikes in East Greenland (Holwell et al., 2012). The morphology of the globular texture may help to decipher the mechanisms of transportation and concentration of sulfide liquid and the distribution of ore types in Ni sulfide deposits (Godel, 2013).

In the Piaohechuan no. 4 Ni-Cu-(PGE) sulfide-bearing intrusion, we found globular ores as well as network and breccia ores. The globular ores are quite similar to those described in the Uruguayan dike swarm and the Sudbury Complex. In this study, we use a combination of petrographic observation, olivine geochemistry, whole-rock lithophile-chalcophile trace elements, and Sr-Nd-Os isotopes to explore the origin of the magmas and sulfides in the Piaohechuan no. 4 intrusion. We

† Corresponding author: e-mail, wang_yan@gig.ac.cn

Submitted: February 2, 2015
Accepted: June 8, 2015

focus on the textures of the ores and provide evidence that sulfide liquid invaded partially molten silicates. We then discuss how this process may have operated to produce the different types of sulfide ores in the intrusion.

Geologic Background

The Central Asian orogenic belt lies between the Siberian craton to the north and the Tarim and North China blocks to the south (Fig. 1a) and formed during subduction of the paleo-Asian oceanic lithosphere that resulted in multistage accretion of island arcs, accretionary wedges, and microcontinents (Windley et al., 2007; Xiao et al., 2009). The paleo-Asian ocean finally closed in the Late Permian (~250 Ma) and the Solonker-Xra Moron-Changchun suture zone in northeastern China marks the termination of the Central Asian orogenic belt (Wu et al., 2007). During the Triassic, this belt underwent a postcollisional extension, resulting in extensive emplacement of mafic-ultramafic intrusions and A-type granitoid plutons (Wu et al., 2011).

The Hongqiling-Piaohechuan region in the easternmost part of the Central Asian orogenic belt is one of the most important regions in China for economic Ni-Cu-(PGE) sulfide mineralization. There are nearly 200 mafic-ultramafic intrusions in this region, which have been dated at between 216 ± 5 and 239 ± 3 Ma using the SHRIMP zircon U-Pb technique (Wu et al., 2004; Hao et al., 2013). These intrusions were emplaced into Paleozoic gneiss, schist, and marble of the Hulan Formation. Only eight intrusions have been found to contain economic Ni-Cu-(PGE) sulfide deposits (Lü et al., 2007). The largest one of these is the Hongqiling no. 7 intrusion, which contains 204,400 metric tons (t) Ni and 39,000 t Cu (Lü et al., 2011) and was the second largest Ni producer after the Jinchuan mine in China (Chai et al., 2003) before mining of the Ni deposits in the Xinjiang province started a few years ago. The Hongqiling no. 7 intrusion is mainly composed of orthopyroxenite and almost the entire intrusion is mineralized. The sulfide ores have an average grade of 2.31 wt % Ni, and the bulk sulfide ores (recalculated to100% sulfide) have average PGE concentrations of 5.6 ppb Os, 3.1 ppb Ir, 4.7 ppb Ru, 2.2 ppb Rh, 31 ppb Pt, and 11 ppb Pd on average (Wei et al., 2013).

The Piaohechuan no. 4 intrusion (Fig. 1b) contains 10,000 t of Ni and 4,000 t of Cu, and the sulfide ores have an average grade of 0.83 wt % Ni (Lü et al., 2007). The intrusion has a surface exposure of ~0.07 km², trending 310° and dipping southwest (Fig. 2a). In plan view, it is lenticular, ~630 m long and 40 to 250 m wide (Fig. 2b). In cross section, the intrusion is shown to be composed of hornblende-olivine gabbro (53 vol %) overlainby hornblende gabbro (47 vol %), and it varies in thickness from 50 to 150 m (Fig. 2c). Sulfide mineralization mainly occurs in the hornblende-olivine gabbro and the hornblende gabbro is generally sulfide barren (Jilin Bureau of Geology and Mineral Resources, 1980). The orebody is exposed in the southeastern part of the intrusion and the main orebody at the base of the hornblende-olivine gabbro is ~430 m long, 40 to 165 m wide, and 4 to 32 m thick. The orebody is thickest (32 m) along exploration line 7 and becomes progressively thinner to the northwest and southeast. The ore penetrates as veins into the footwall gneiss along exploration lines 11 and 3 (Fig. 2c).

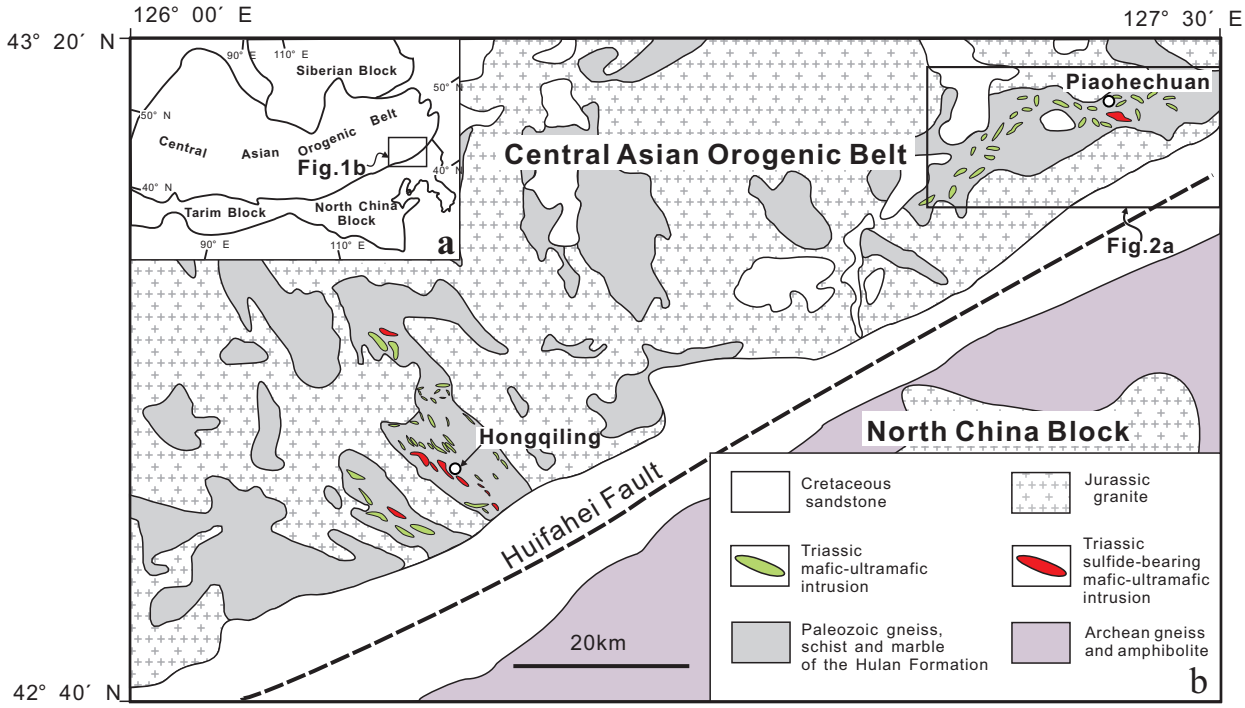

FIG. 1. (a). A simplified geologic map of the Central Asian orogenic belt (modified from Xiao et al., 2009). (b). A map showing the distribution of the Triassic mafic-ultramafic intrusions along the Huifahe fault in the Hongqiling-Piaohechuan region (modified from Wu et al., 2004).

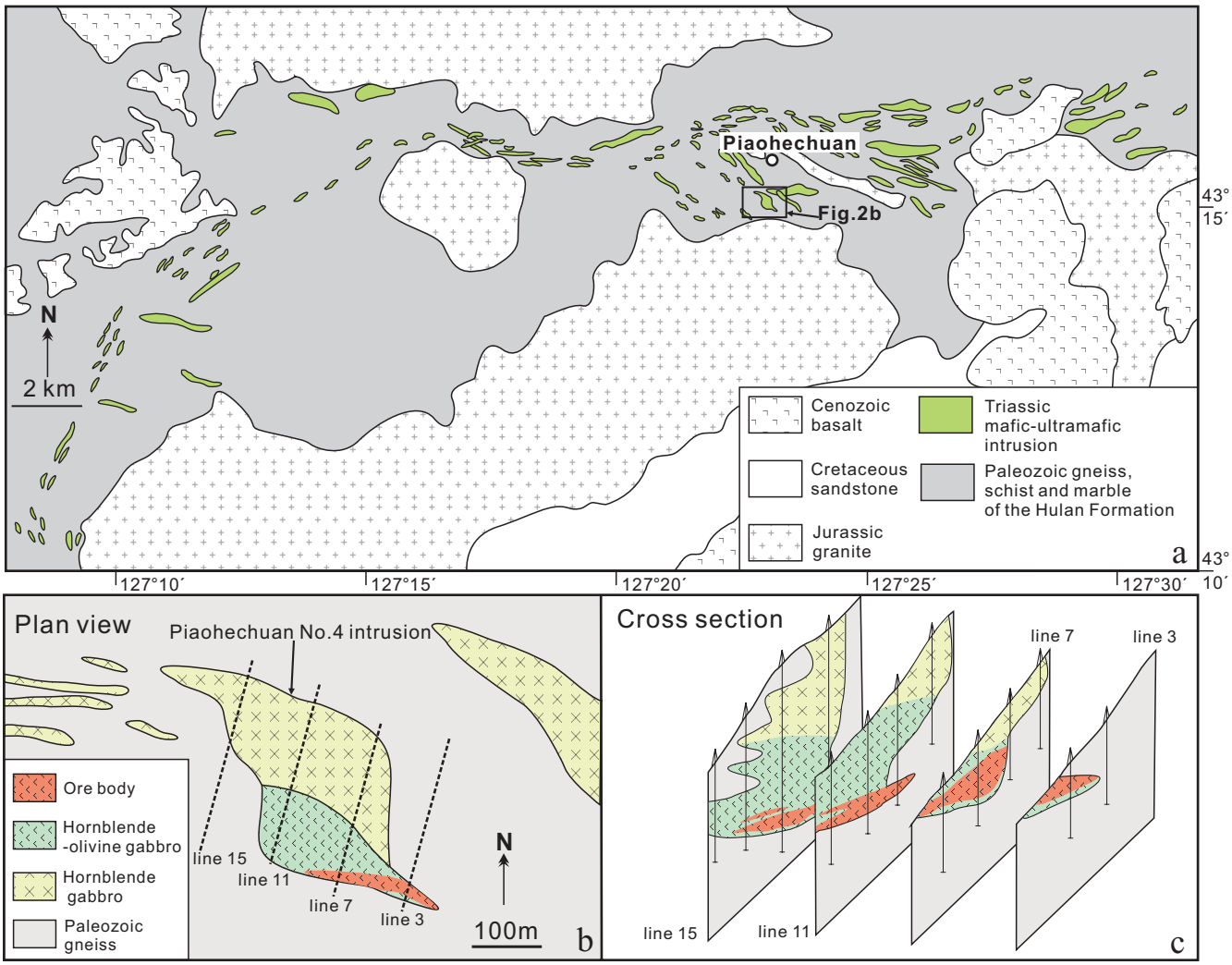

FIG. 2. (a). A simplified geologic map showing the distributions of mafic-ultramafic intrusions in the Piaohechuan region (modified from Wu et al., 2004). (b). Plan view of the Piaohechuan no. 4 intrusion. (c). Cross section of the Piaohechuan no. 4 intrusion (modified from Wu et al., 2004 and Jilin Bureau of Geology and Mineral Resources, 1980).

Petrography

Host rocks

The hornblende-olivine gabbro in the lower portion of the intrusion contains pre-alteration proportions of 10 to 15 modal % olivine, 25 to 35% clinopyroxene, 10 to 15% orthopyroxene, 20 to 30% plagioclase, and 5 to 10% hornblende with minor biotite (Fig. 3a). Due to intensive alteration, olivine is partially or totally replaced by serpentine, clinopyroxene crystals are partially or totally altered to tremolite (Fig. 3a, d), orthopyroxene has altered to talc (Fig. 3a), plagioclase is partially or totally altered to sericite. Primary brown hornblende that is partially replaced by pale green chlorite at the rim, survives as relics (Fig. 3b), with the tremolite pseudomorphous after the original mafic minerals. The shapes and sizes of the magmatic minerals described below are mainly based on the distributions of the secondary mineral pseudomorphs. Olivine grains are anhedral to subhedral and vary in size from 0.2 to 0.6 mm in diameter and have Fo contents ranging from 72 to 86 (Table 1). Olivine grains are commonly enclosed in either hornblende or plagioclase (Fig. 3a, b). Some olivine grains contain small, rounded sulfide blebs (Fig. 3c). Clinopyroxene (now tremolite) occurs as discrete crystals with diameters ranging from 0.1 to 0.3 mm. Orthopyroxene (totally altered into talc) occurs either as granular crystals with diameters ranging from 0.2 to 0.6 mm, or intergranular crystals between olivine grains. Plagioclase commonly occurs as medium-grained, tabular crystals. Hornblende and biotite occupy the angular interstices between olivine and pyroxene grains (Fig. 3a, b). The inferred crystallization sequence based on the textures is olivine → clinopyroxene → orthopyroxene → plagioclase + hornblende + biotite.

Fine- to medium-grained hornblende gabbro in the upper portion of the intrusion originally contained about 40 to 50% clinopyroxene, 25 to 35% plagioclase, and 10 to 15% hornblende, with minor biotite, apatite, and Fe-Ti oxides. Fine-grained dolerite occurs at the margin of the intrusion with a similar mineral assemblage to the hornblende gabbro (Fig. 3d).

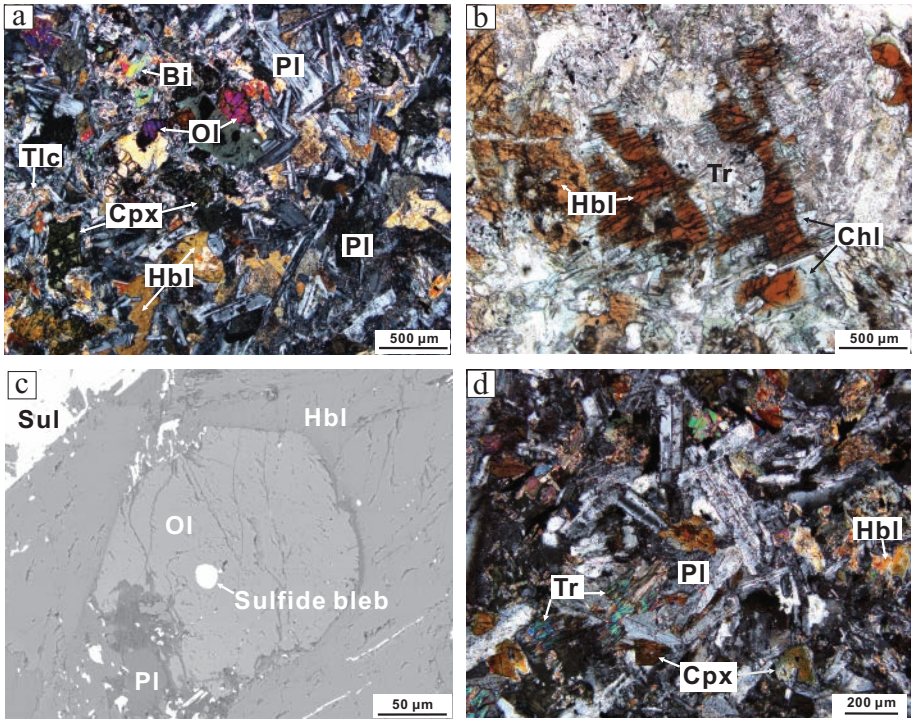

FIG. 3. Microphotographs of hornblende-olivine gabbro in the Piaohechuan no. 4 intrusion. (a). Hornblende-olivine gabbro is mainly composed of olivine (Ol), clinopyroxene (Cpx), orthopyroxene which is totally altered into talc (Tlc), plagioclase (Pl), hornblende (Hbl), and minor biotite (Bi) (under cross-polarized and transmitted). (b). The brown hornblende is relic and partially replaced by pale green chlorite(Chl) on the rim, with tremolite (Tr) pseudomorphous after the primary mafic minerals (underplane-polarizer and transmitted). (c). A small, rounded sulfide (Sul) bleb enclosed in olivine (BSE image). (d). Fine-grained dolerite occurs at the margin of the intrusion and some of the pyroxene grains are altered into tremolite (under cross-polarized and transmitted).

Sulfide ores

Three types of sulfide ores in the intrusion were described in the mine reports as semimassive, net-textured, and disseminated (Jinline Bureau of Geology and Mineral Resources, 1980), which are normally used to describe textures in Ni-Cu-(PGE) sulfide deposits. However, these terms are not appropriate for the sulfide ores of the Piaohechuan no. 4 intrusion. In deposits such as Jinchuan and those of the Kambalda and Noril'sk camps, the term "massive" applies to ore containing close to 100% sulfide, "net-textured" refers to ore in which cumulus crystals with magmatic morphologies are surrounded by an interconnected matrix of sulfide, and "disseminated" refers to a rock with small grains or patches of sulfide that are isolated and interstitial to silicate minerals. For the sulfide ores of the Piaohechuan 4 intrusion, we propose the following terms:

"Globular" ore: This ore resembles certain disseminated sulfide ore textures from the Black Swan deposit in the Yilgarn craton (Barnes et al., 2009), the Sudbury Complex (Naldrett, 1969; Pattison, 1979), or the Noril'sk-Talnakh deposits (Arndt et al., 2003). As shown in Figure 4a, this type contains large patches or globules containing almost 100% sulfide in rock otherwise almost devoid of sulfide. The sulfides are mainly pyrrhotite (80–88 vol %) and pentlandite (10–11 vol %) with anhedral grains or intergrowths of chalcopyrite (5–7 vol %; Fig. 4b).

The globules are 2 to 10 mm across and vary in shape from spherical to irregular (Fig. 4a, c, d). Most globules consist of 100% sulfide, but several contain inclusions of gabbroic rock. The external borders of the globules themselves are in contact with the grains of relatively coarse-grained hornblende or plagioclase (Fig. 4d). One inclusion of gabbroic rock in the globule shown in Figure 4e is almost spherical and its perfectly rounded border has a brown hornblende grain on the left and a plagioclase grain on the right. The border of the other inclusion in Figure 4e has concave portions, in contrast with the protruding boundary of sulfide in contact with the gabbro inclusion. Projecting from the margin of the spherical globule (Fig. 4d) are crystals of tremolite (Fig. 4f), a secondary mineral that appears to have grown into the sulfide.

"Network" ore: This ore superficially resembles the "net-textured" ore of other deposits in that the relative proportions of sulfide and silicate minerals are similar. However, rather than forming an interconnected matrix enclosing cumulus olivine crystals in a net-textured ore, in network ore the sulfide forms what appear in two dimensions to be irregular tube-like channels with cuspate margins at contacts with the silicate rocks (Fig. 5a, b). The channels are 1 to 2 mm wide and they can be followed discontinuously in thin section for tens of millimeters. Along their length the channels pinch and swell to produce bulbous nodes that are connected by narrower, more rectilinear segments (Fig. 5c). The sulfides in the channels are pyrrhotite (83–91 vol %), pentlandite (8–11 vol %), and chalcopyrite (1–7 vol %). The sulfide is rich in Cu

Table 1. Compositions of Olivine Grains in the Breccia Ores in the Piaohechuan No. 4 Intrusion

Sample no.	PH-3									
Points	1	2	3	4	5	6	7	8	9	10
SiO_2 (wt %)	38.58	39.25	39.07	39.92	38.99	38.82	39.42	39.52	39.27	37.70
MgO	37.29	43.53	38.51	42.14	38.99	37.13	38.78	40.58	40.04	37.58
FeO	23.48	15.58	21.58	17.79	21.10	23.58	21.69	20.22	20.82	21.76
CaO	0.03	0.08	0.16	0.28	0.02	0.07	0.07	0.03	0.03	0.13
MnO	0.42	0.26	0.37	0.30	0.38	0.48	0.38	0.32	0.33	0.35
Cr_2O_3	0.02	0.03	0.00	0.05	0.07	0.00	0.07	0.00	0.02	0.06
NiO	0.08	0.17	0.09	0.20	0.09	0.13	0.07	0.15	0.16	0.14
Total	99.82	98.73	99.69	100.47	99.55	100.08	100.41	100.67	100.50	97.57
Fo (mol %)	73.6	83.1	75.8	80.6	76.4	73.3	75.8	77.9	77.1	75.18
Ni (ppm)	589	1,297	723	1,579	715	990	581	1,210	1,257	1,124

Sample no.	PH-4									
Points	11	12	13	14	15	16	17	18	19	20
SiO_2 (wt %)	39.76	38.96	40.65	38.91	40.22	38.97	39.32	38.83	39.11	38.19
MgO	43.54	39.43	46.22	43.08	43.86	38.78	41.13	38.74	40.48	36.13
FeO	16.36	21.83	13.60	16.55	15.54	22.02	19.07	22.08	20.54	25.17
CaO	0.12	0.04	0.14	0.02	0.21	0.06	0.08	0.04	0.25	0.09
MnO	0.25	0.37	0.17	0.31	0.28	0.41	0.36	0.45	0.35	0.49
Cr_2O_3	0.04	0.03	0.06	0.05	0.08	0.06	0.04	0.00	0.07	0.00
NiO	0.21	0.10	0.25	0.17	0.28	0.15	0.13	0.06	0.11	0.05
Total	100.06	100.66	100.84	98.91	100.18	100.30	100.00	100.12	100.80	100.06
Fo (mol %)	82.4	76.0	85.7	82.0	83.2	75.5	79.1	75.4	77.6	71.5
Ni (ppm)	1,682	778	1,988	1,297	2,208	1,179	1,045	440	833	393

Sample no.	PH-4							PH-6		
Points	21	22	23	24	25	26	27	28	29	30
SiO_2 (wt %)	39.68	38.41	38.62	39.27	38.17	39.07	39.26	39.59	38.90	40.42
MgO	44.20	37.65	41.24	41.87	39.63	43.41	39.99	42.08	40.12	43.82
FeO	15.91	24.00	19.00	18.11	21.94	17.37	21.63	18.07	18.34	14.33
CaO	0.02	0.08	0.08	0.02	0.06	0.04	0.05	0.10	0.06	0.11
MnO	0.24	0.42	0.29	0.33	0.44	0.26	0.41	0.27	0.32	0.19
Cr_2O_3	0.02	0.00	0.00	0.03	0.08	0.00	0.00	0.00	0.02	0.06
NiO	0.24	0.11	0.18	0.12	0.20	0.08	0.08	0.22	0.14	0.23
Total	100.08	100.57	99.23	99.61	100.33	100.15	101.34	100.33	97.89	99.17
Fo (mol %)	83.0	73.3	79.2	80.2	75.9	81.4	76.4	80.6	79.6	84.5
Ni (ppm)	1,886	857	1,375	904	1,556	652	652	1,699	1,061	1,842

Sample no.	PH-6								
Points	31	32	33	34	35	36	37	38	39
SiO_2 (wt %)	39.99	38.37	39.57	40.79	38.21	38.70	40.42	38.85	39.33
MgO	42.19	39.17	43.32	45.05	39.15	41.33	44.92	40.06	42.72
FeO	17.42	21.87	17.29	14.09	21.99	19.23	15.13	21.21	17.54
CaO	0.04	0.04	0.10	0.33	0.12	0.08	0.08	0.05	0.05
MnO	0.30	0.42	0.29	0.22	0.43	0.26	0.27	0.28	0.29
Cr_2O_3	0.11	0.21	0.03	0.00	0.08	0.06	0.00	0.00	0.02
NiO	0.14	0.08	0.18	0.29	0.15	0.17	0.26	0.14	0.17
Total	100.19	100.17	100.78	100.77	100.13	99.82	101.08	100.59	100.13
Fo (mol %)	81.2	76.2	81.7	85.1	76.0	79.3	84.1	77.1	81.3
Ni (ppm)	1,133	638	1,399	2,258	1,211	1,298	2,028	1,077	1,305

in local places, where the sulfides are pyrrhotite (80 vol %), chalcopyrite (13 vol %), and pentlandite (7 vol %). Chalcopyrite commonly forms networks of tiny veins filling in cracks in silicate minerals (Fig. 5d).

The contacts between sulfide and silicate minerals of the fresh gabbro are sharp but smoothly rounded (Fig. 5e). In many samples, the host rock is altered to secondary minerals (tremolite, talc, and chlorite), and in such cases the contacts, and the overall form of the networks, are irregular (Fig. 5f). In places the host rock is highly fractured, fine veins of sulfide fill these fractures, and small angular fragments of silicate minerals (hornblende or plagioclase) are enclosed in a sulfide matrix (Fig. 5f).

"Breccia" ores: These ores occur in the lower part of the main orebody near the base of the intrusion. None of the samples contains 100% sulfide; all contain numerous fragments from the host intrusion (Fig. 6a). In breccia ores, the proportion of fragments varies from about 10 to 50%, at which point it grades into network ore. The size of the fragments varies from several microns to about 2 cm. The sulfides enclosing the fragments are pyrrhotite (85–90 vol %), pentlandite (8–11 vol %), and chalcopyrite (<3 vol %).

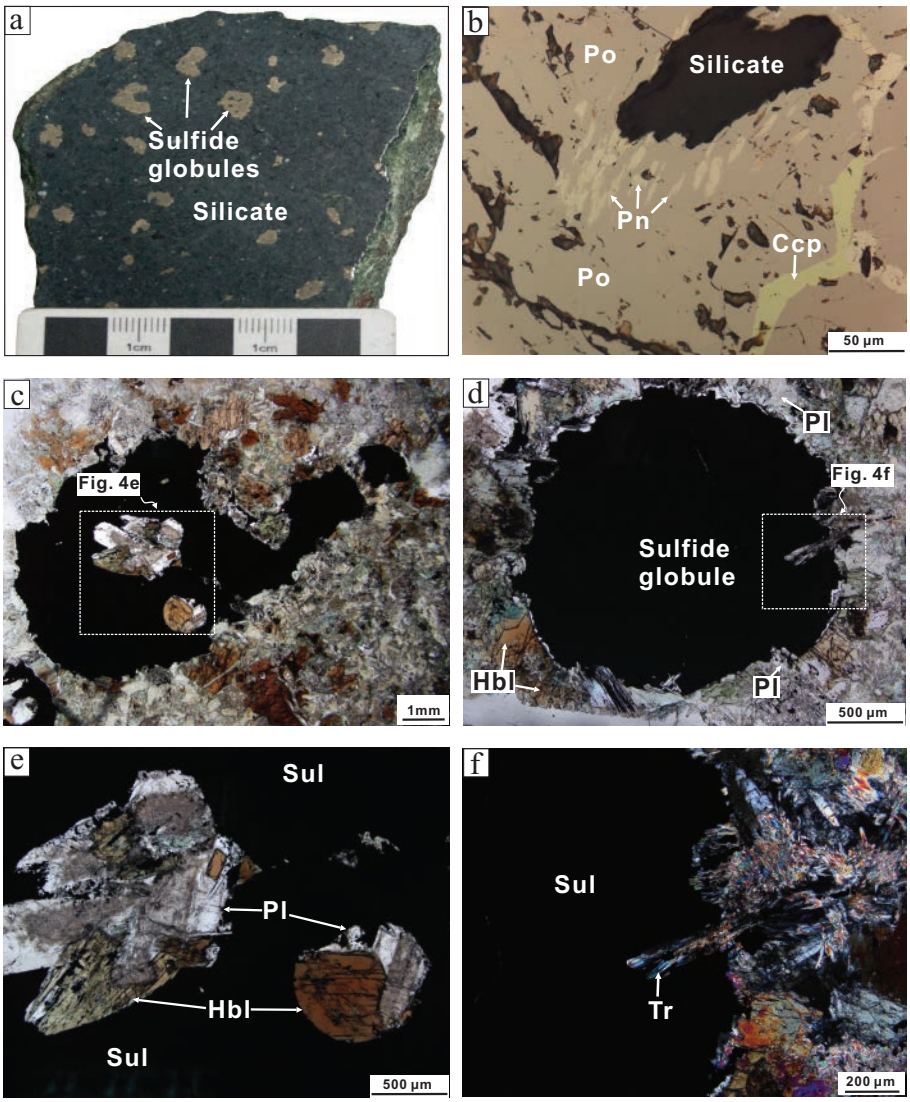

FIG. 4. Textures of globular ore. (a). A hand specimen showing irregular or rounded sulfide globules in silicate. (b). The globule is composed of pyrrhotite (Po), pentlandite (Pn), and chalcopyrite (Ccp). Pentlandite occurs as flame in pyrrhotite (under reflected light). (c). An irregular globule enclosing two inclusions of gabbroic rocks (under cross-polarized and transmitted). (d). An almost spherical sulfide globule in contact with relatively coarse grained hornblende and plagioclase (under cross-polarized and transmitted). (e). Close-up of (c). Note the rounded form of the smaller inclusion and the concave boundary of the gabbro inclusion (under cross-polarized and transmitted). (f). Close-up of (d) (under cross-polarized and transmitted). Abbreviations as in Figure 3.

The fragments consist of broken pieces of rock, or individual medium- to coarse-grained crystals, from the host intrusion (Fig. 6b-f). The rock fragments have magmatic textures and mineral assemblages like those of the host intrusion, consisting of olivine, orthopyroxene (altered into talc and chlorite), plagioclase, and hornblende (Fig. 6b). Some fragments are single grains, mainly of hornblende and plagioclase and in some cases fresh clinopyroxene or olivine. Their angular form and their contacts with the sulfide matrix cut across twinning and other crystallographic features (Fig. 6c). Some adjacent fragments of plagioclase have almost continuous twin planes (Fig. 6d).

The rock fragments in some thin sections display a diversity of textures: most fragments consist of coarse-grained gabbro, but some are much smaller in size with a doleritic texture, resembling the marginal phases of the intrusion (right side, Fig. 6e). In some breccias the fragments have magmatic textures, but the mineral assemblage is entirely secondary like that of most rocks in the intrusion, for example, the fragments are altered to talc and chlorite (Fig 6e). Only the fragments enclosed within a sulfide matrix are fresh—rocks from the rest of the intrusion are totally altered except for some relic hornblende (Fig. 6f). When the rock is altered, the fragments are less compact and far less regular in form and size.

Of particular significance are the embayments and rounded borders of the fragments of gabbro, which resemble the contacts of the sulfide channels in network ores (Fig. 6g, h). Figure 7 illustrates a whole thin section with an intact gabbroic texture and a transition from the network ore on the left to the breccia ore on the right.

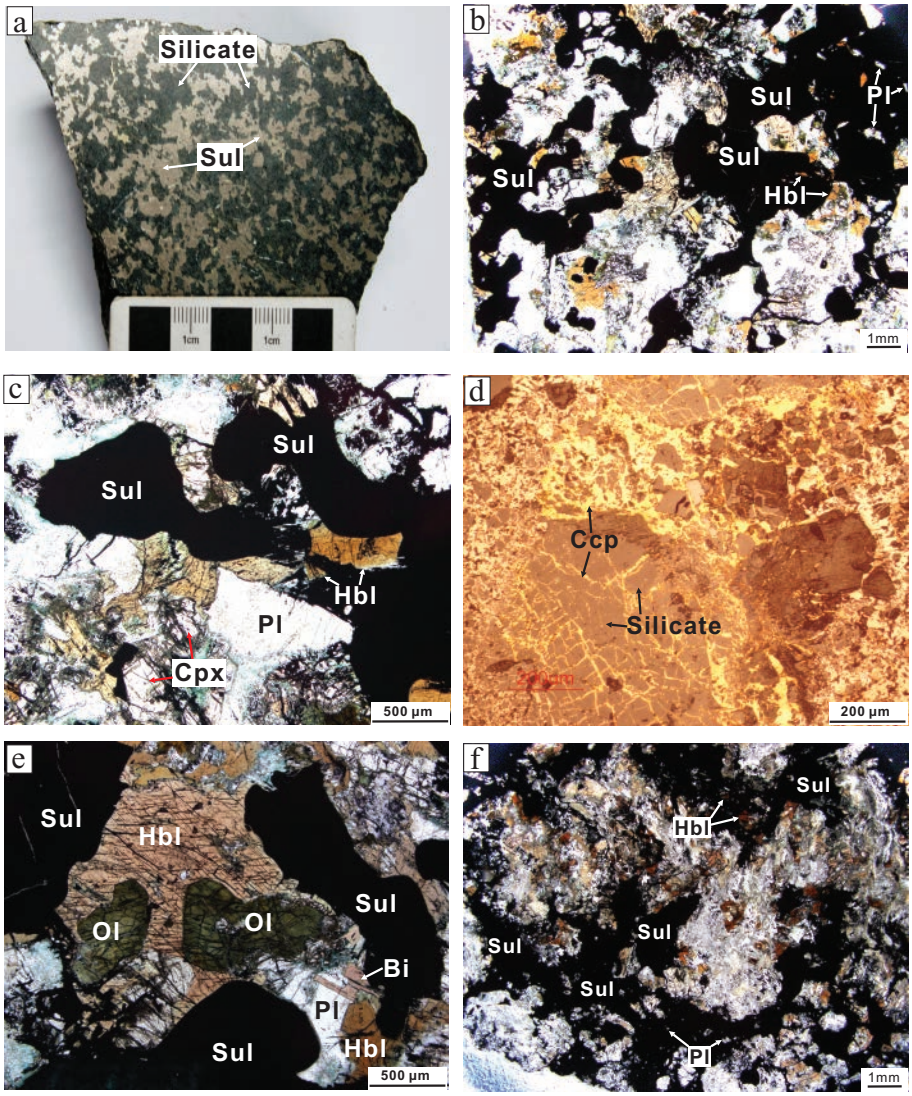

FIG. 5. Textures of network ore. (a). Hand specimen of network ore showing that the irregular sulfides are intergrown with the silicate rocks. (b). Sulfides form tube-like channels and have cuspate margins in the contact with partially altered gabbro (under plane-polarizer and transmitted). (c). Sulfide shows bulbous nodes and narrower intervening segments (under plane-polarizer and transmitted). (d). Chalcopyrite veins fill in the cracks in gabbro (under reflected light). (e). Sulfide and silicate show rounded contacts (under plane-polarizer and transmitted). (f). A far more irregular network of sulfides and altered gabbro (under plane-polarizer and transmitted). Abbreviations as in the Figures 3 and 4.

Platinum-group minerals (PGM) and PGE-bearing minerals

A total of 17 PGM grains have been identified from three breccia and two network ore samples. They include 14 grains of michenerite (PdTeBi) and three grains of sperrylite ($PtAs_2$). In addition, eight PGE-bearing cobaltite [(CoNiFe)AsS] grains have been identified in these samples (Table 2).

Euhedral and subhedral sperrylite crystals are 3 × 1 to 12 × 6 μm in size and are enclosed either in pyrrhotite (Fig. 8a, b) or cobaltite (Fig. 8c). They are stoichiometric in composition and contain 52.8 to 56.8 wt % Pt and 42.2 to 44.2 wt % As (Table 2).

Irregular michenerite grains are associated with chalcopyrite and fill cracks in chalcopyrite (Fig. 8d). These michenerite grains range in size from 2 × 2 to 15 × 3 μm. They have compositions of 22.6 to 25.7 wt % Pd, 30.2 to 31.9 wt % Te, and 42.4 to 45.2 wt % Bi (Table 2).

Euhedral to subhedral cobaltite grains range from 2 × 2 to 20 × 15 μm in diameter. Most cobaltite grains are enclosed in pyrrhotite (Fig. 8e, f) and contain 1.6 to 18.3 wt % Ir, 1.6 to 6.2 wt % Pt, and 4.4 to 10.2 wt % Rh. The PGE-bearing parts of the cobaltite appear as bright spots when viewed in a BSE image (Fig. 8e). One small cobaltite grain is PGE bearing throughout the whole grain (Fig. 8f).

Whole-Rock Compositions

Major elements

Samples from the Piaohechuan no. 4 intrusion have variable loss-on-ignition (LOI) of 2.89 to 14.3 wt % (Table 3) due to variable degrees of alteration. They have S contents ranging from 2.8 to 34.5 wt % (Table 4). The sulfide-bearing samples have been normalized on a volatile- and sulfide-free basis, and

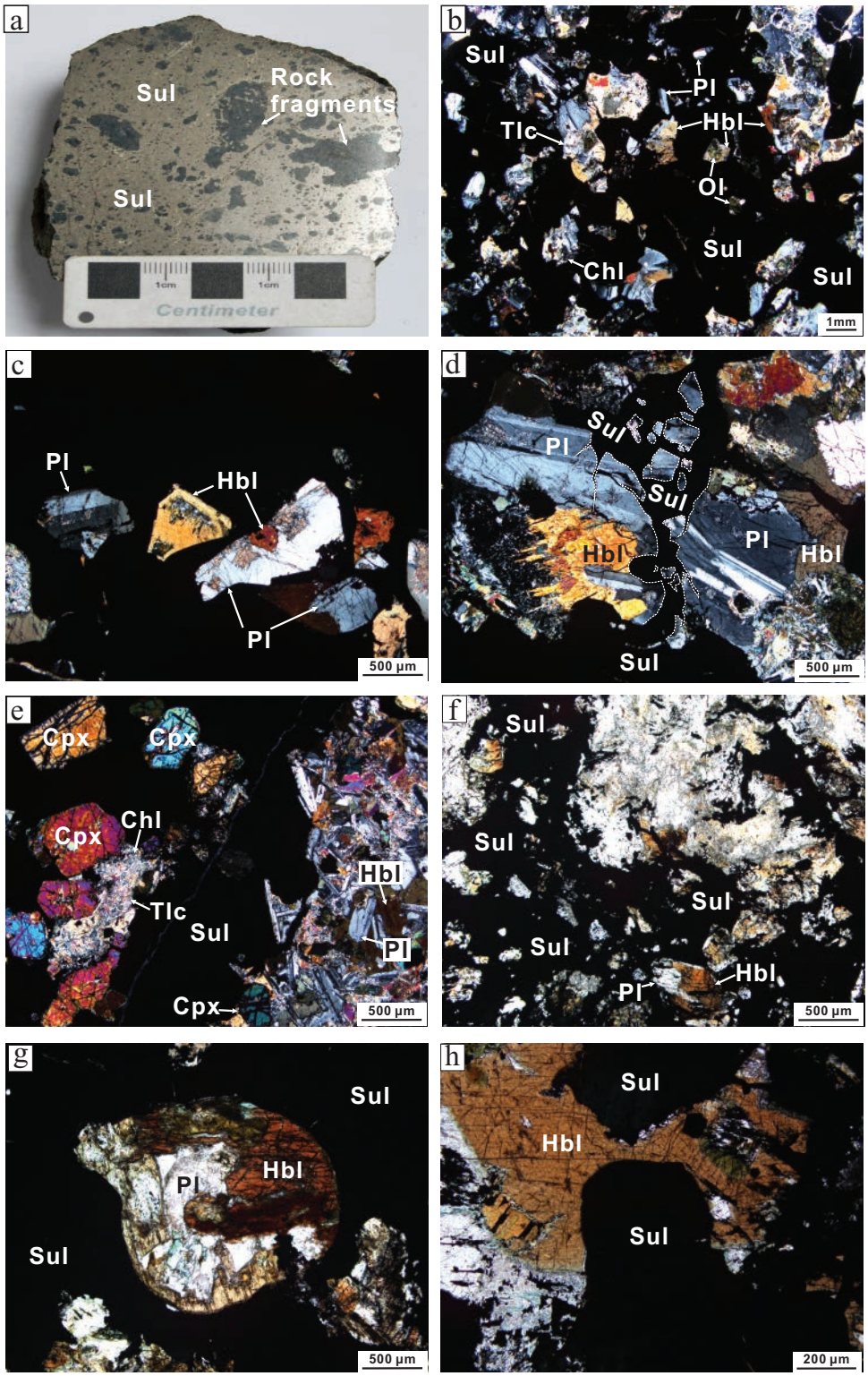

FIG. 6. Textures of breccia ore. (a). Hand specimen of breccia ore showing that irregular rock fragments are enclosed in sulfide. (b). Fragments of the breccia have similar mineral assemblages to the host gabbro. Pyroxene is altered into talc and chlorite (under cross-polarized and transmitted). (c). Broken crystals of plagioclase and hornblende enclosed in sulfide. Note the truncated twin planes in the plagioclase grain (under cross-polarized and transmitted). (d). Several fragments of gabbro that are minimally displaced, as shown by almost continuous twin planes of the plagioclase (under cross-polarized and transmitted). (e). Isolated, almost entire, clinopyroxene grains on the left and a large fragment of fine-grained dolerite on the right (under cross-polarized and transmitted). (f). An irregular network of sulfide and highly altered gabbro (under plane-polarizer and transmitted). (g). A rounded fragment of gabbro enclosed in sulfide (under cross-polarized and transmitted). (h). The embayment textures in a hornblende grain (under cross-polarized and transmitted).

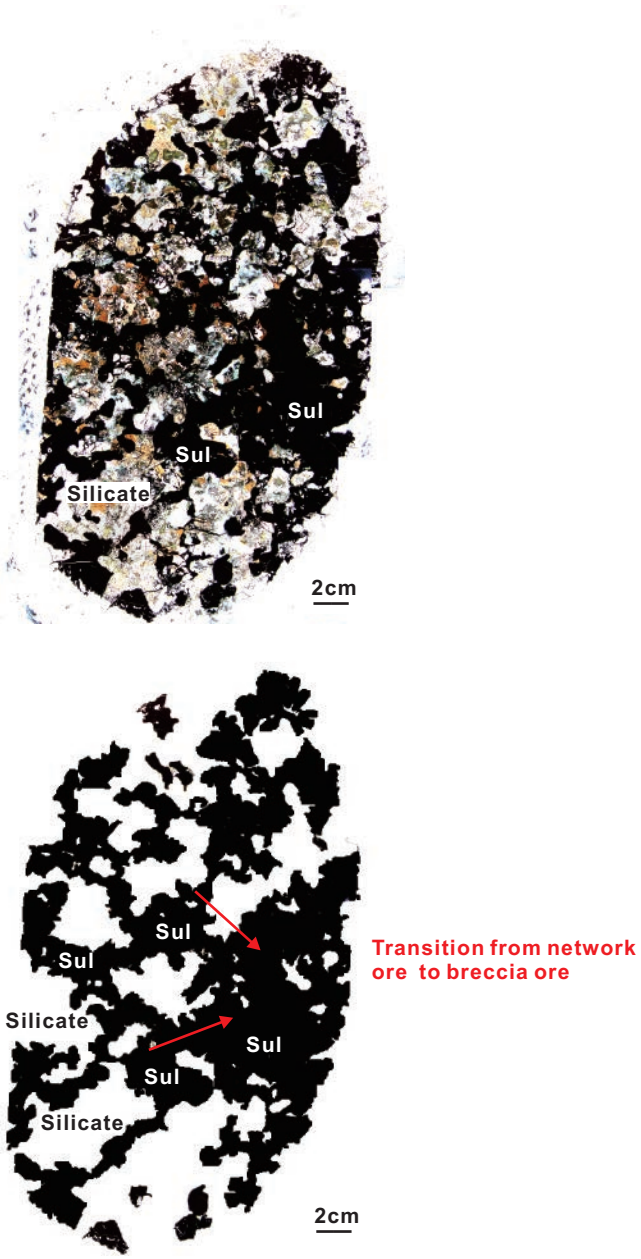

FIG. 7. A mosaic of the thin section (PH-3), showing a transition from network ore, above, to breccia ore, below. The rock fabric remains intact.

FeO_{total} has been corrected for Fe in FeS. Sulfide contents have been estimated for sulfide-bearing samples based on the S, Ni, and Cu content of the samples, using the procedure described by Naldrett and Duke (1980) and documented in detail by Li et al. (2001). The amount of Ni in the bulk sulfide was corrected after allowing for a contribution from silicate minerals, using an average Ni concentration of 600 ppm for S-poor samples.

PGE, Cu, Ni, and S

All the sulfide ore samples show a good correlation between Ni and S (Fig. 9a), indicating an approximately constant Ni

TABLE 2. Representative Normalized Compositions (wt %) of Platinum-Group Minerals and PGE-Bearing Cobaltite in the Breccia and Network Ores in the Piaohechuan No. 4 Intrusion

Ore type	Host	Shape	Pd	Pt	Ir	Rh	Fe	Co	Ni	Cu	Te	Bi	As	S	Total	Co#[1]	Atomic formula[2]
Sperrylite																	
Cu-rich network ore	Pyrrhotite	Anhedral		52.8			4.1						42.2	0.9	100.0		$(Pt_{0.87}Fe_{0.23})_{1.1}(As_{1.8}S_{0.09})_{1.9}$
Cu-rich network ore	Pyrrhotite	Anhedral		55.8									44.2		100.0		$PtAs_2$
Network ore	Cobaltite	Anhedral		56.8									43.2		100.0		$Pt_{1.01}As_{1.99}$
Michenerite																	
Breccia ore	Chalcopyrite	Anhedral	22.6				1.1			0.9	30.2	45.2			100.0		$(Pd_{0.91}Fe_{0.09}Cu_{0.06})_{1.06}(Bi_{0.93}Te_{1.01})_{1.94}$
Breccia ore	Chalcopyrite	Anhedral	23.2				1.7				30.7	44.4			100.0		$(Pd_{0.93}Fe_{0.13})_{1.06}(Bi_{0.91}Te_{1.03})_{1.94}$
Breccia ore	Chalcopyrite	Anhedral	25.7								31.9	42.4			100.0		$Pd_{1.04}(Bi_{0.88}Te_{1.08})_{1.96}$
Network ore	Chalcopyrite	Anhedral	24.7								30.9	44.5			100.0		$Pd_{1.01}(Bi_{0.93}Te_{1.06})_{1.99}$
Network ore	Chalcopyrite	Anhedral	24.4								31.6	44.0			100.0		$Pd_1(Bi_{0.92}Te_{1.08})_2$
PGE-bearing cobaltite																	
Breccia ore	Pyrrhotite	Euhedral		1.6	1.6	1.3	6.7	16.8	7.9				45.8	18.2	100.0	0.7	$(Co_{0.49}Ni_{0.23}Fe_{0.21}Rh_{0.02}Ir_{0.01}Pt_{0.01})As_{1.06}S_{0.97}$
Breccia ore	Pyrrhotite	Euhedral		1.7	2.0	1.0	7.5	16.9	8.9				44.2	17.8	100.0	0.7	$(Co_{0.49}Ni_{0.26}Fe_{0.23}Rh_{0.02}Ir_{0.02}Pt_{0.02})_{1.04}As_{1.01}S_{0.95}$
Breccia ore	Pyrrhotite	Euhedral		6.2		0.7	10.2	16.9	6.2				40.0	19.7	100.0	0.7	$(Co_{0.49}Ni_{0.18}Fe_{0.31}Rh_{0.01}Pt_{0.05})_{1.04}As_{0.91}S_{1.05}$
Network ore	Pyrrhotite	Euhedral		4.2	17.8	2.4	5.1	11.2	5.2				38.1	16.2	100.0	0.7	$(Co_{0.38}Ni_{0.17}Fe_{0.18}Ir_{0.18}Rh_{0.05}Pt_{0.04})_1As_1S_1$
Network ore	Pyrrhotite	Euhedral		4.7	18.1	1.8	5.0	10.6	5.5				38.0	16.1	100.0	0.6	$(Co_{0.35}Ni_{0.19}Fe_{0.18}Ir_{0.19}Rh_{0.04}Pt_{0.05})_1As_1S_1$
Network ore	Pyrrhotite	Euhedral		4.1	16.0	1.3	5.8	11.2	5.9				39.8	16.0	100.0	0.6	$(Co_{0.37}Ni_{0.2}Fe_{0.2}Ir_{0.16}Rh_{0.02}Pt_{0.04})_{0.99}As_{1.04}S_{0.97}$
Network ore	Pyrrhotite	Euhedral		2.7	10.5	0.6	5.4	12.8	8.0				42.6	17.4	100.0	0.7	$(Co_{0.4}Ni_{0.25}Fe_{0.17}Ir_{0.1}Rh_{0.01}Pt_{0.03})_{0.96}As_{1.04}S_1$
Network ore	Pyrrhotite	Euhedral			13.3	2.6	4.4	15.9	4.3				42.1	17.4	100.0	0.8	$(Co_{0.5}Ni_{0.14}Fe_{0.15}Ir_{0.13}Rh_{0.04})_{0.96}As_{1.04}S_1$
Network ore	Pyrrhotite	Euhedral			8.9	3.2	5.1	15.9	5.3				43.8	17.7	100.0	0.8	$(Co_{0.49}Ni_{0.16}Fe_{0.16}Ir_{0.08}Rh_{0.06})_{0.95}As_{1.06}S_{0.99}$
Network ore	Pyrrhotite	Euhedral		3.4	12.2	3.2	4.5	14.3	5.1				40.3	17.0	100.0	0.7	$(Co_{0.46}Ni_{0.17}Fe_{0.15}Ir_{0.12}Rh_{0.06}Pt_{0.03})_{0.99}As_{1.01}S_1$

[1] Cobaltite-gersdorffite series calculated by Co# = Co/(Co + Ni) (atomic)
[2] Atomic formula calculated on three atoms

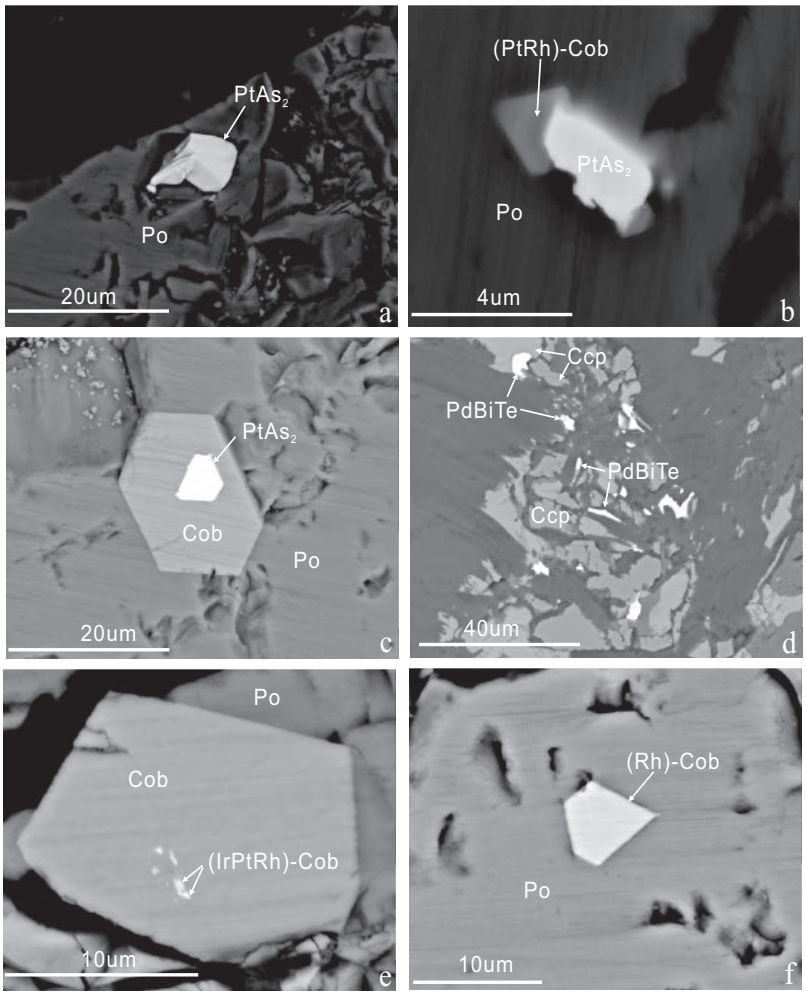

FIG. 8. BSE images of platinum-group minerals (PGM) and PGE-bearing minerals in breccia and network ores. (a). An euhedral sperrylite($PtAs_2$) grain enclosed in pyrrhotite (Po) in breccia ore. (b). A sperrylite grain which is adjacent to an euhedral PGE-rich cobaltite (Cob) enclosed in pyrrhotite in breccia ore. (c). An euhedral sperrylite crystal enclosed in a larger euhedral PGE-poor cobaltite in network ore. (d). Michenerite (PdBiTe) is associated with chalcopyrite (Ccp) in network ore. (e). Euhedral cobaltite grains with distinct faces enclosed in pyrrhotite in network ore, and the light area of the cobaltite is PGE rich. (f). A whole cobaltite grain in breccia that is PGE rich.

tenor (concentration in 100% sulfide) of around 3 wt % and a poor correlation between Cu and S (Fig. 9b). They show a positive correlation of S with Ir and Ru (Fig. 9c, d) except for the only one sample of Cu-rich network ore, and they show no correlation of S with Pt or Pd (Fig. 9e, f). Ni_{100} (Ni in 100% sulfides) has no correlation with Pt_{100} and Pd_{100} (Fig. 10a, c). Cu_{100} shows a weak positive correlation with Pd_{100} but no correlation with Pt_{100} (Fig. 10b, d). Ir_{100} shows a good positive correlation with Ru_{100} (Fig. 10e), except for the one Cu-rich network ore sample, but shows poor negative correlations with Pt or Pd (Fig. 10f , g). There is no correlation between Pt_{100} and Pd_{100} (Fig. 10h). Breccia, network, and globular ores have Pd/Ir ratios ranging from 0.7 to 24 and Pd/Pt ratios from 0.23 to 31, whereas the Cu-rich network ore has a Pd/Ir ratio of 73 and a Pd/Pt ratio of 1.1.

Breccia ores have lower PPGEs (Rh, Pt, and Pd) than network and globular ores (Fig. 11a, b, d) and highly variable Pt concentrations so that they have either weak positive (in a few samples) or (more commonly) very negative Pt anomalies in the primitive mantle-normalized chalcophile element patterns (Fig. 11a). Network and globular ores have generally similar PGE patterns (Fig. 11b, d). Some network ores have negative Pt anomalies (Fig. 11b). The sample of Cu-rich network ore has negative Os and Ru anomalies (Fig. 11c) and depletion of all the IPGEs (Os, Ir, and Ru) relative to Ni.

Sr-Nd and Re-Os isotope compositions

Samples from the Piaohechuan no. 4 intrusion have relatively constant $^{143}Nd/^{144}Nd$ ratios, ranging from 0.51258 to 0.51259. They have εNd (t = 216 Ma) values from 4.4 to 4.6 (Table 5). However, their initial $^{87}Sr/^{86}Sr$ (t = 216 Ma) ratios are variable from 0.7057 to 0.7065, which define an array that is distinctly displaced to the right of the mantle array (Fig. 12).

Sulfide ores contain 20 to 161 ppb Re and 2.2 to 24.7 ppb Os. They have $^{187}Re/^{188}Os$ ratios ranging from 26.25 to 52.30 and $^{187}Os/^{188}Os$ ratios from 0.2908 to 0.3748. The initial $^{187}Os/^{188}Os$ (t = 216 Ma) ratios of the ores range from 0.1748

TABLE 3. Major Oxide Compositions (wt %) of the Rocks and Sulfide Ores in the Piaohechuan No. 4 Intrusion

Sample no.	SiO_2	Al_2O_3	TiO_2	Fe_2O_3	FeO	MnO	MgO	CaO	Na_2O	K_2O	P_2O_5	LOI
Breccia ore												
PH-1	11.12	2.76	0.25	36.50	25.00	0.08	4.06	1.45	0.36	0.21	0.07	11.08
PH-2	4.87	1.16	0.11	63.89	8.82	0.05	0.85	0.10	0.20	0.20	0.05	14.34
PH-3	14.02	3.34	0.31	27.81	30.32	0.10	4.61	1.79	0.60	0.26	0.08	10.11
PH-4	20.45	4.70	0.38	21.47	27.30	0.14	7.90	2.59	0.80	0.35	0.11	8.47
PH-6	16.88	4.19	0.34	23.68	28.49	0.11	5.90	3.30	0.63	0.27	0.10	9.64
PH-7	14.72	3.63	0.30	40.76	16.96	0.11	4.84	1.92	0.60	0.27	0.07	10.10
PH-9	18.98	4.38	0.40	32.83	17.98	0.11	6.96	2.53	0.59	0.45	0.11	9.87
PH-10	20.87	4.50	0.38	34.23	14.08	0.10	8.52	2.80	0.46	0.41	0.10	9.46
PH-13	19.43	4.03	0.32	33.06	16.74	0.11	8.82	2.40	0.42	0.29	0.09	9.90
PH-14	18.96	4.17	0.36	34.27	17.40	0.10	7.06	2.22	0.52	0.33	0.10	10.07
Network ore												
PH-11	25.85	5.51	0.44	28.47	11.76	0.14	11.56	2.97	0.39	0.38	0.12	8.88
PH-12	25.89	5.55	0.42	32.68	8.60	0.14	10.65	2.35	0.45	0.53	0.12	9.18
PH-15	26.77	5.66	0.47	28.42	10.22	0.13	11.18	3.61	0.35	0.47	0.13	9.11
PH-16	36.46	7.07	0.58	9.03	10.80	0.16	16.25	4.53	0.30	0.31	0.17	10.85
PH-17	30.70	5.96	0.48	22.60	9.87	0.14	14.78	3.61	0.40	0.20	0.14	7.98
Cu-rich network ore												
PH-5	23.23	6.27	0.32	34.24	8.46	0.17	7.70	4.07	1.00	0.44	0.11	7.47
Globular ore												
PH-8	40.98	10.28	0.85	8.68	9.09	0.16	13.06	6.57	1.49	0.81	0.22	6.10
PH-18	41.58	8.46	0.67	5.88	10.36	0.16	18.28	5.71	0.99	0.99	0.19	5.06
PH-19	41.49	7.82	0.57	6.92	10.14	0.16	19.47	4.92	0.56	0.68	0.18	5.33
Sulfide-poor hornblende-olivine gabbro												
PH-20	48.24	11.85	1.36	2.53	8.13	0.15	13.62	5.21	2.64	2.17	0.44	2.89

TABLE 4. Sulfur Contents and Chalcophile Element Concentrations of the Sulfide Ores in the Piaohechuan No. 4 Intrusion

Sample no.	S (wt %)	Ni (ppm)	Os (ppb)	Ir (ppb)	Ru (ppb)	Rh (ppb)	Pt (ppb)	Pd (ppb)	Cu (ppm)
Breccia ore									
PH-1	29.0	25,124	22.7	20.2	22.0	22.0	19.1	74.4	1,670
PH-2	34.5	28,936	35.0	26.9	30.3	22.5	21.6	18.0	1,020
PH-3	26.9	22,269	34.6	24.8	29.3	20.8	1.72	34.1	1,186
PH-4	21.7	18,211	25.6	21.3	25.9	16.4	2.49	37.7	6,030
PH-6	17.8	19,579	33.4	24.2	30.0	18.9	69.5	31.2	4,122
PH-7	26.2	21,936	29.3	25.6	29.1	20.8	2.86	89.5	2,206
PH-9	22.9	18,526	34.9	22.1	27.2	18.7	134	37.6	551
PH-10	21.2	17,667	30.0	20.3	25.1	17.1	7.22	41.9	1,522
PH-13	22.0	18,673	28.6	21.4	26.1	16.5	190	43.3	2,051
PH-14	23.0	17,904	29.4	22.3	26.8	17.7	89.5	55.5	1,342
Network ore									
PH-11	16.3	15,284	17.9	11.8	14.8	9.42	6.47	41.0	3,718
PH-12	16.5	14,235	14.2	10.4	12.4	8.60	155	42.4	5,766
PH-15	15.8	16,020	15.7	10.6	13.1	8.88	50.8	46.9	2,083
PH-16	5.21	5,226	3.62	2.49	3.30	2.24	56.1	58.7	3,352
PH-17	11.8	12,312	8.77	6.69	8.76	6.07	205	46.9	1,069
Cu-rich network ore									
PH-5	24.76	17,407	3.64	5.26	2.56	9.23	343	383	29,297
Globular ore									
PH-8	3.57	4,344	3.02	2.83	3.19	2.54	44.0	29.8	2,323
PH-18	2.80	3,340	2.21	1.78	2.25	1.50	44.4	20.5	1,207
PH-19	2.94	3,815	2.45	1.89	2.25	1.58	57.9	19.3	1,547

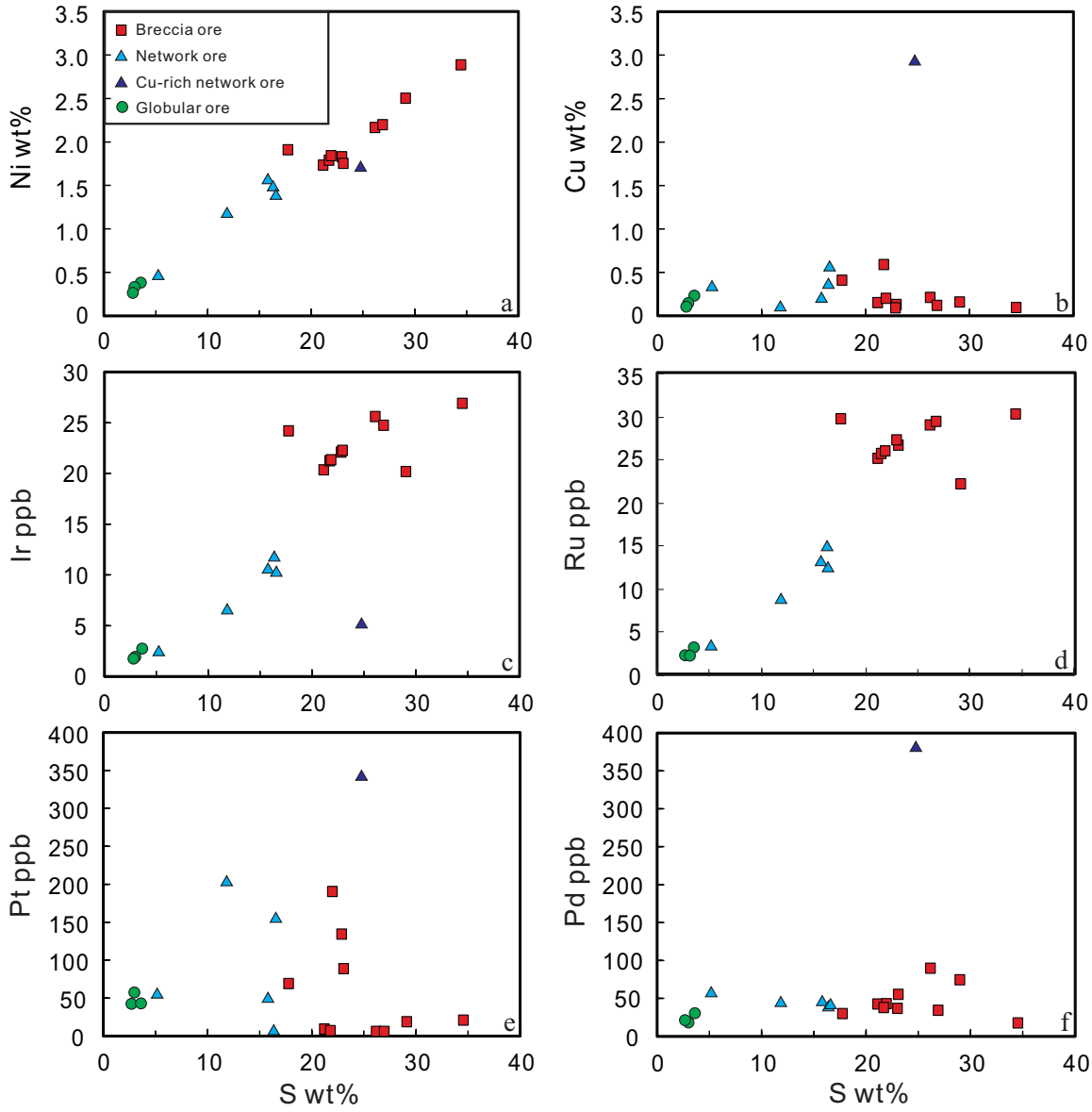

FIG. 9. Variations of Ni (a), Cu (b), Ir (c), Ru (d), Pt (e), and Pd (f) with S content in the sulfide ores in the Piaohechuan no. 4 intrusion.

to 0.2096, corresponding to γ_{Os} (t = 216 Ma) values varying from 39 to 67 (Table 6).

Discussion

Variations of PGE affected by magmatic process and hydrothermal alteration

Fractionation of sulfide liquid involves segregation of Ni- and IPGE-rich liquidus monosulfide solid solution (mss) and a Cu- and PPGE-rich residual melt, which eventually solidifies to an assemblage dominated by intermediate solid solution (iss; Barnes and Maier, 1999). The breccia, network, and globular ores of the Piaohechuan no. 4 intrusion probably formed from mss-enriched cumulates because they are relatively enriched in Ni, Os, Ir, and Ru and have good correlations of S with Ni, Ir, and Ru (Fig. 9a, c, d) and poor correlations of S with Pt and Pd (Fig. 9e, f). The Cu-rich network ore is rare in this intrusion and the Cu-rich ore sample has much higher Cu, Pt, and Pd and lower Os, Ir, and Ru than other ores (Fig. 11) and may have formed from residual Cu-rich liquid in local places.

The variation of Pt that produces positive and negative anomalies on the primitive mantle-normalized chalcophile patterns for the breccia and network ore (Fig. 11a, b) is likely to be associated with the affinity of Pt for arsenic. This has led to the formation of sperrylite, which occurs sporadically in the ores and also occurs in the centers of crystals of cobaltite. The cobaltite belongs to the sulfarsenide solid solution series composed of cobaltite-gersdorffite-arsenopyrite, in which Co exchanges for Ni and Fe, respectively (Hem and Makovicky, 2004). The composition of this solid solution is often used to estimate the minimum temperature of its formation using the

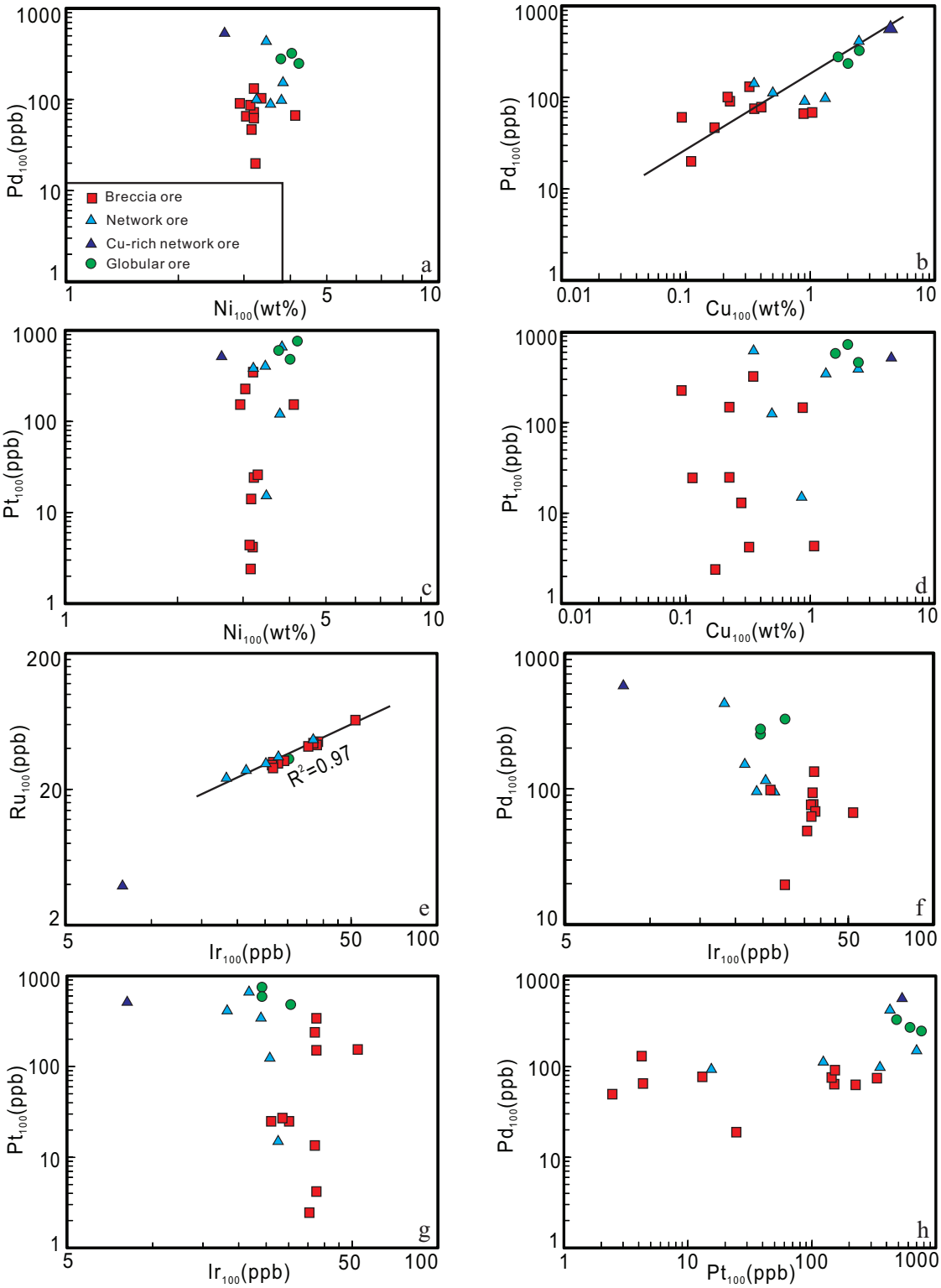

FIG. 10. Interelemental relationships between PGE, Ni, and Cu in recalculated 100% sulfide for the sulfide ores in the Piaohechuan no. 4 intrusion. The trend lines are linear regression lines. R is the correlation coefficient.

experimental results of Klemm (1965). In the Piaohechuan no. 4 intrusion, the compositions of the euhedral cobaltite grains in the breccia ores are consistent with a minimum temperature of ~550°C (Fig. 13), similar to those described elsewhere (Hanley, 2007; Godel et al., 2012; Prichard et al., 2013). The sperrylite inclusions in the central part of some euhedral cobaltite grains are considered to have crystallized from a PGE- and As-bearing sulfide liquid at a very high

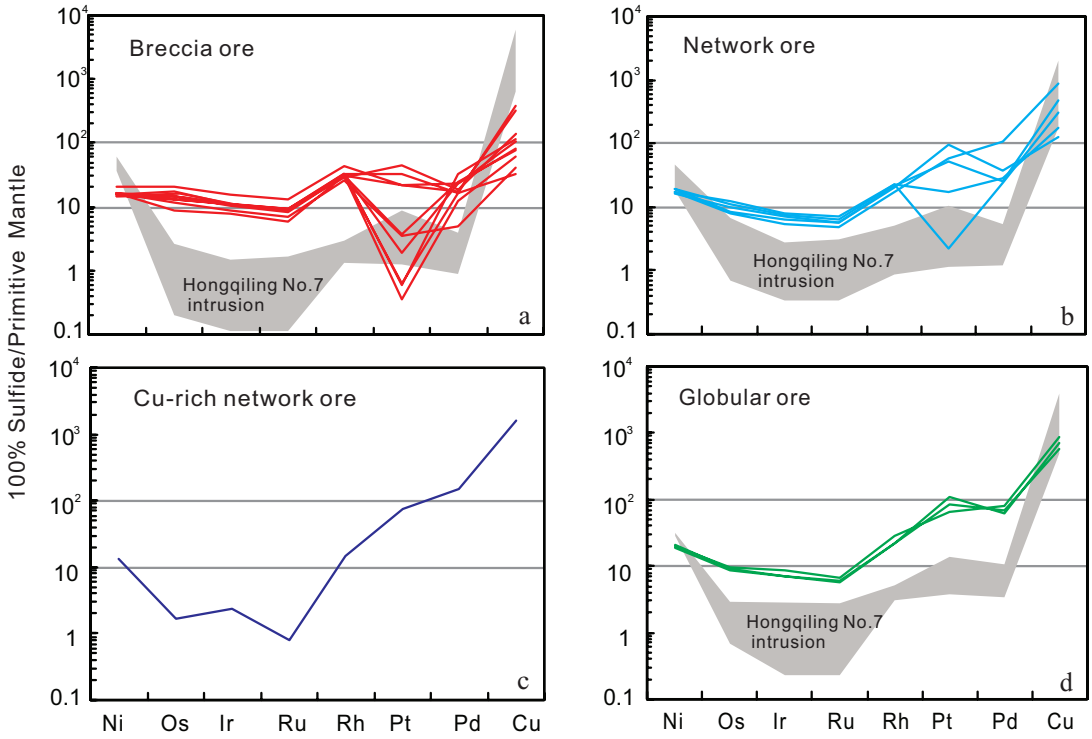

FIG. 11. Primitive mantle-normalized chalcophile element patterns for the sulfide ores in the Piaohechuan no. 4 intrusion. The shadow area is inferred to the sulfide ores of the Hongqiling no. 7 intrusion (data from Wei et al., 2013). The concentrations are recalculated to 100% sulfide. Normalizing values are from Barnes and Maier (1999).

temperature (~1,200°C, Wood, 2003; Dare et al., 2010), prior to the crystallization of mss (1,000°–1,040°C, Fleet et al., 1993). This is likely to be the case for the sperrylites observed in this study (Fig. 8c).

The locations of the PGM indicate that subsequent hydrothermal alteration has not remobilized the PGE to any great extent. The sperrylite inclusions may have been preserved in the centers of the cobaltite crystals (Fig. 8b, c) and so shielded from remobilization during subsequent hydrothermal alteration. The intergrowth of sulfide and needle-like tremolite and vein-like chalcopyrite along the cracks in the silicates of the network ores (Fig. 5d) are direct evidence for overprinted hydrothermal alteration. Michenerite is believed to have formed due to the exsolution of Pd from chalcopyrite during hydrothermal alteration (e.g., Dare et al., 2010). Michenerite is present in the Cu-rich network ore in the Piaohechuan no. 4 intrusion and is also likely to have exsolved from the chalcopyrite. However, the most altered Cu-rich network ore has a Pd/Pt ratio of 1.1, similar to many sulfide ores with a magmatic origin (Barnes and Lightfoot, 2005). In the Cu-rich network ore, the michenerite grains are observed to be associated closely with chalcopyrite (Fig. 8d), indicating that Pd was not mobilized far from the chalcopyrite by hydrothermal fluids. We therefore consider that the hydrothermal alteration did not modify the PGE concentrations in the sulfide ores of the Piaohechuan no. 4 intrusion.

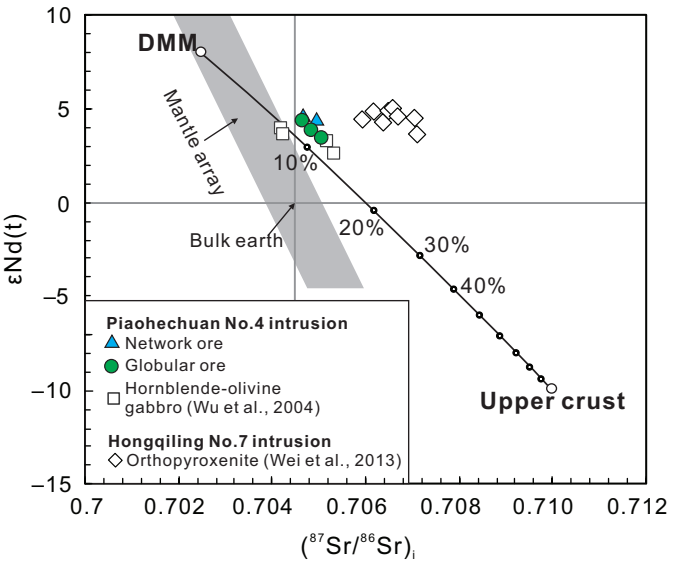

FIG. 12. Plot of $\varepsilon_{Nd(total)}$ values and $(^{87}Sr/^{86}Sr)_i$ ratios showing the degrees of crustal contamination for the rocks and sulfide ores in the Piaohechuan no. 4 and Hongqiling no. 7 intrusions. Data sources: D-MORB (Zindler and Hart, 1986); upper crust (Rudnick and Gao, 2003).

A high-Mg basaltic parental magma

Os, Ir, Ru, and Ni are more compatible in the mantle than Pd, Pt, and Cu during partial melting so that komatiite has a Ni/Cu ratio of 12 to 16 (Barnes, 2006), much higher than that of basalt of 1 to 10, and a Pd/Ir ratio of 0.2 to 10, much lower than that of basalt of 10 to 20 (Barnes and Maier, 1999). The network and breccia ores of the Pioahechuan no. 4 intrusion have much larger variations of Ni/Cu ratio than that of the globular ore, due to the fractionation of sulfide liquid and

TABLE 5. Rb-Sr and Sm-Nd Isotope Compositions of the Sulfide Ores in the Piaohechuan No. 4 Intrusion

Sample no.	Rb (ppm)	Sr (ppm)	$^{87}Rb/^{86}Sr$	$^{87}Sr/^{86}Sr$	Error (2σ)	$(^{87}Sr/^{86}Sr)_i$	Sm (ppm)	Nd (ppm)	$^{147}Sm/^{144}Nd$	$^{143}Nd/^{144}Nd$	Error (2σ)	$(^{143}Nd/^{144}Nd)_i$	$\varepsilon_{Nd(t)}$
Breccia ore													
PH-9	11.32	72.59	0.4514	0.706063	0.000014	0.70467	1.83	7.86	0.1409	0.512795	0.000011	0.51259	4.6
PH-13	6.67	63.26	0.3049	0.705926	0.000013	0.70499	1.57	6.85	0.1390	0.512784	0.000010	0.51259	4.5
Network ore													
PH-11	10.53	58.83	0.5178	0.706472	0.000011	0.70487	2.53	11.38	0.1348	0.512775	0.000012	0.51258	4.4
Globular ore													
PH-18	25.18	216.74	0.3362	0.705675	0.000013	0.70464	4.18	17.88	0.1414	0.512789	0.000013	0.51259	4.5

Notes: Initial ratios were calculated using the age of 216 Ma

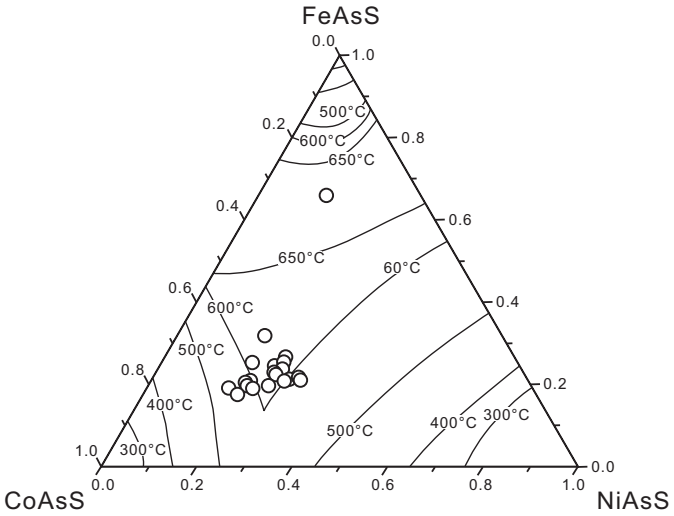

FIG. 13. Ternary phase diagram of sulfarsenide solid-solution series (CoAsS-FeAsS-NiAsS), showing that the formation temperature of the cobaltite in the Piaohechuan no. 4 intrusion is above 500°C. Temperature data are after Klemm (1965).

remobilization of Cu during hydrothermal processes. The Ni/Cu and Pd/Ir ratios of less fractionated globular ore samples are used to infer the composition of parental magma, which have Ni/Cu of 1.6 to 2.3 and Pd/Ir of 10.2 to 11.5, similar to those derived from high Mg basaltic magmas elsewhere (Fig. 14).

Wu et al. (2004) used the average composition of less fractionated dolerite and gabbro samples in the intrusions to estimate the parental magma of the mafic-ultramafic intrusions in the Piaohechuan region. The estimated parental magma contains 48.2 wt % SiO_2, 10.9 wt % MgO, and an Mg # of 0.67 (Wu et al., 2004). This composition is that of a tholeiitic magma with a moderate MgO content. If we assume that the MgO/FeO ratio that we measured in olivine is the same as that of the olivine that crystallized from the magma, the composition of the parental magma of the Piaohechuan no. 4 intrusion can be estimated using the most magnesian olivine composition and the olivine-liquid Fe-Mg exchange coefficient (K_D), $(FeO/MgO)_{Ol}/(FeO/MgO)_{magma} = 0.3$ (Roeder and Emslie, 1970). The most magnesian olivine in the Piaohechuan no. 4 intrusion has Fo content of 85.8 (Table 1), which corresponds to a Mg # of 0.65, essentially the same as the estimate of Wu et al. (2004).

The highest Fo content (85.8) of olivine in the Piaohechuan no. 4 intrusion is much lower than that of mantle olivine (Fo >90), indicating that the olivine crystallized from a relatively evolved magma. If we assume that olivine is the first phase that crystallized from the primary magma, the composition of the primary magma (i.e., the composition of the mantle partial melt that subsequently evolved to become the parental magma of the intrusion) can be estimated by incrementally adding olivine with Fo content varying from 85.8 to 90 to the evolved magma (Li et al., 2012) until the composition of the magma is in equilibrium with olivine of Fo_{90}, the estimated composition of the mantle olivine. The total amount of olivine added to the magma is constrained by the K_D value (0.3).The back calculation gives 15.5 wt % MgO for the primary magma.

TABLE 6. Re-Os Isotope Compositions of the Sulfide Ores in the Piaohechuan No. 4 Intrusion

Sample no.	Re (ppb)	Os (ppb)	$^{187}Re/^{188}Os$	2σ	$^{187}Os/^{188}Os$	2σ	$(^{187}Os/^{188}Os)_i$	$\gamma_{Os(t = 216\ Ma)}$
Breccia ore								
PH-1	75	14.02	26.25	0.0360	0.2908	0.0005	0.1962	56
PH-2	131	18.45	34.90	0.5000	0.3117	0.0008	0.1858	48
PH-3	118	19.42	29.96	0.1480	0.3041	0.0012	0.1961	56
PH-7	162	24.69	32.30	3.3000	0.3043	0.0004	0.1880	50
PH-9	140	23.33	29.55	0.0640	0.2968	0.0005	0.1902	52
PH-10	132	20.06	32.40	0.1000	0.3008	0.0006	0.1839	46
PH-13	142	22.74	30.80	0.0812	0.3014	0.0006	0.1904	52
Network ore								
PH-11	75	14.02	26.25	0.0360	0.2908	0.0005	0.1962	56
PH-12	105	11.32	46.10	0.1000	0.3523	0.0007	0.1862	48
PH-16	30	3.10	47.75	0.0948	0.3748	0.0007	0.2026	61
PH-17	80	7.63	52.30	0.6000	0.3632	0.0009	0.1748	39
Cu-rich network ore								
PH-5	32	3.18	49.27	0.3300	0.3737	0.0035	0.1961	56
Globular ore								
PH-18	20	2.20	45.22	0.1157	0.3726	0.0009	0.2096	67
PH-19	22	2.45	43.99	0.0532	0.3428	0.0009	0.1842	47

Note: γ_{Os} (t = 216 Ma) values were calculated using the Os evolution curve of the chondritic mantle

Note that this value represents the maximum value because concurrent crustal contamination may have occurred. The true value should be between 10.9 and 15.5 wt %, which is within between a picritic and high Mg basaltic magma and requires high degrees of partial melting of the mantle (O'Hara, 1968; Naldrett, 2010). This value is similar to the MgO content (11–16 wt %) of the primary magma estimated for the Hongqiling no. 7 intrusion in the same region (Wei et al., 2013), indicating that these two intrusions may have originated from similar primary magma.

Crustal contamination or derivation from metasomatized lithospheric mantle?

Whole-rock trace elements and Nd, Sr, and Os isotopes provide some constraints on the mantle source. The intrusion is inferred to have formed during a period of rifting following closure of the paleo-Asian ocean (Wu et al., 2004). There is no evidence of a mantle plume and therefore the likely source was the ambient asthenosphere or the lithospheric mantle. The asthenosphere would have had a moderately depleted composition with low Th/Nb and low Nb/La (Sun and McDonough, 1989); if the lithospheric mantle had been metasomatized during subduction it may have had negative Nb-Ta anomalies expressed as high Th/Nb and low Nb/La (Saunders et al., 1991). Rocks from the Piaohechuan no. 4 intrusion display negative Nb-Ta anomalies: their $(Th/Nb)_{PM}$ ratios range from 3 to 11, significantly higher than the mid-ocean ridge basalt (MORB) or ocean-island basalt (OIB), and their $(Nb/La)_{PM}$ ratios from 0.11 to 0.39, lower than the OIB (Fig. 15, Table 7). These values can be explained either by contamination with rocks from the continental crust or by derivation from a metasomatized lithospheric mantle.

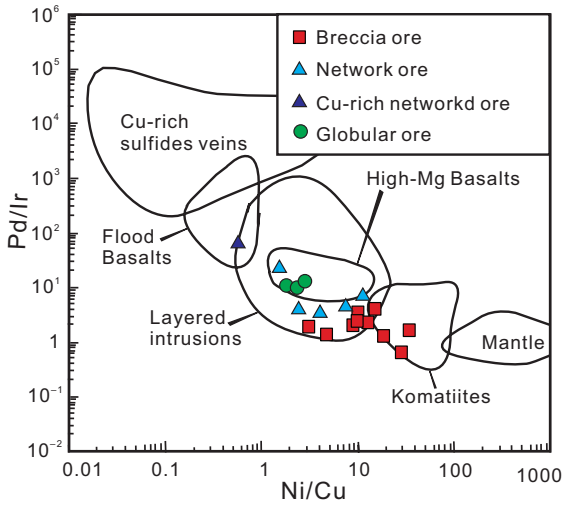

FIG. 14. A plot of Pd/Ir vs. Ni/Cu ratios for the sulfide ores in the Piaohechuan no. 4 intrusion. Reference fields are after Barnes and Lightfoot (2005).

The rocks of the Piaohechuan no. 4 and Hongqiling no. 7 intrusions have positive $\varepsilon_{Nd(t)}$ values (4.4–4.6 and 3.1–5.0; Fig. 12), suggesting that the crustal component, whether in the mantle source or an assimilate, had short crustal residence time. However, the Sr and Os isotope compositions are highly radiogenic. There are three possible interpretations: (1) these values result from alteration; (2) they are the characteristics of the subduction component that had moderate $\varepsilon_{Nd(t)}$ and high $^{87}Sr/^{86}Sr$ values, like the Banda arc volcanics(Vroon et al., 1993); and (3) these were the characteristics of crustal material that was assimilated to the magma. Final distinction between these components will require analysis of the isotopic compositions of the rocks from the region. However, we prefer the crustal contamination model for the following reasons: (1) Os is thought to be less mobile than Sr (Walker et al., 1989) and high γ_{Os} values are not reported in subduction-related magmas (McInnes et al., 1999); (2) sulfur is highly soluble in relatively oxidized magmas from subduction settings than in rift settings and such magmas would need to assimilate large amounts of a reductant before sulfide can segregate (Thakurta et al., 2008). There is no evidence of such a

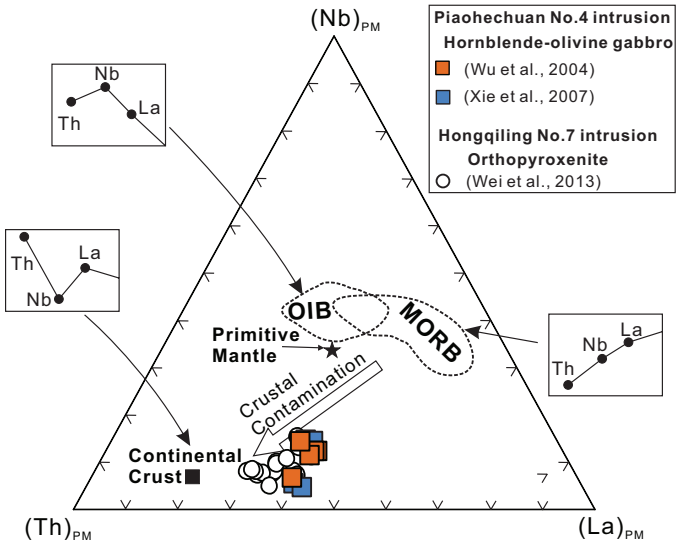

FIG. 15. La-Nb-Th diagram showing that the samples from the Piaohechuan no. 4 intrusion are along the crustal contamination trend. Reference fields are after Jochum et al. (1991). All data are normalized to primitive mantle values from Sun and McDonough (1989).

process in the region. We thus propose that the geochemical features of the Piaohechuan no. 4 and Hongqiling no. 7 intrusions resulted from the assimilation of relatively young A-type granite in this region.

This process was also considered to have triggered sulfide saturation due to elevation of SiO_2 content in the parental magma, resulting in minor amounts of sulfide segregated in the deep-seated magma chamber so that the parental magma of the Piaohechuan no. 4 and Hongqiling no. 7 intrusions is PGE depleted (Wei et al., 2013). The parental magma of the Hongqiling no. 7 intrusion is estimated to contain 0.04 ppb Os, 0.03 ppb Ir, and 0.1 ppb Pd after previous segregation of ~0.2% immiscible sulfide liquid at depth (Wei et al., 2013). We consider that the Piaohechuan no. 4 intrusion may have formed from a parental magma with PGE concentrations similar to the Hongqiling no. 7 intrusion.

Controls on sulfide saturation in a shallow magma chamber

The presence of rounded sulfide droplets in olivine of the Piaohechuan no. 4 intrusion indicates that sulfide saturation was reached prior to or concurrent with olivine crystallization in a shallow magma chamber (Fig. 3c). There is a sharp decrease of Ni concentration in the olivine grains with low Fo content (Fig. 16), consistent with concurrent sulfide saturation. As discussed in "Petrography—PGE, Cu, Ni, and S" section, the primary magma of the intrusion has a composition between picrite and high Mg basalt, and we can assume that the parental magma has about 500 ppm Ni, similar to that of the picrite in the Emeishan large igneous province (Wang et al., 2007). Using this Ni value and assuming that the olivine-magma and sulfide liquid-magma partition coefficients for Ni are 7 (Li et al., 2003) and 400 (Francis, 1990), respectively, modeling results indicate that most olivine grains have Ni concentration that varies with the Fo content along a trend of concurrent olivine crystallization and sulfide segregation (Fig. 16).

The fractionation of olivine may have resulted in the limited sulfide saturation in the Piaohechuan magma chamber. We considered that extensive sulfide saturation may be caused by the addition of external crustal sulfide in the magma chamber. As mentioned earlier, the sulfide ores of the Piaohechuan no. 4 intrusion have restricted $\varepsilon_{Nd(t)}$ values of 4.4 to 4.6, comparable with that of the Hongqiling no. 7 intrusion (3.1–5.0). However, the sulfide ores of both intrusions have variable $\gamma_{Os(t)}$ values; those of the Piaohechuan no. 4 intrusions have $\gamma_{Os(t)}$ values varying from 39 to 67, whereas those of the Hongqiling no. 7 intrusion from 50 to 141 (Fig. 17). The highly variable $\gamma_{Os(t)}$ values coupled with restricted $\varepsilon_{Nd(t)}$ values for the rocks of the Hongqiling no. 7 intrusion were interpreted as a result of the assimilation of crustal sulfide in a shallow magma chamber (Wei et al., 2013). Crustal sulfides are not main carriers of Nd, Sr, and REE but are enriched in Re, so addition of crustal sulfides may not change the $\varepsilon_{Nd(t)}$ values but can significantly elevate the $\gamma_{Os(t)}$ values (Ripley et al., 1999; Lambert et al., 2000; Yang et al., 2012).The sulfide ores of the Piaohechuan no. 4 intrusion have a relatively restricted range of $\gamma_{Os(t)}$ values to those of the Hongqiling no. 7 intrusion, indicating that the assimilation of external crustal sulfide may have also occurred but may have been less significant in the Piaohechuan no. 4 intrusion than in the Hongqiling no. 7 intrusion. An alternative explanation is that the external crustal sulfide may have different Os isotope compositions from those in the Hongqiling no. 7 intrusion. This needs further examination with more Re-Os isotope data of the country rocks in this region.

Interpretation of textures in the sulfide ores

Formation of the globular ore: The globules probably represent coalesced small sulfide droplets that segregated from mafic magma (Fig. 4). The shape of the sulfide droplets was governed by the balance between surface tension and gravity

TABLE 7. A Comparison of Trace Element Ratios and Size Between the Piaohechuan No. 4 and Hongqiling No. 7 Intrusions

Intrusions	$(Th/Nb)_{PM}$	$(Nb/La)_{PM}$	$\varepsilon_{Nd(t)}$	$\gamma_{Os(t)}$	Surface exposure	Size
Piaohechuan no. 4 intrusion	3.2 to11.4	0.11 to 0.39	2.6 to 4.6	39 to 67	0.07 km²	Length: 630 m Width: 180 m (on avg) Extension downward: 180 m
Hongqiling no. 7 intrusion	3.2 to 12.4	0.14 to 0.44	3.1 to 5.0	50 to 187	0.013 km²	Length: 750 m Width: 28 m (on avg) Extension downward: 520 m

Data sources: Trace element ratios of the Piaohechuan no. 4 intrusion are from Wu et al. (2004) and Xie et al. (2007); the data of the Hongqiling no. 7 intrusion are from Wei et al. (2013)

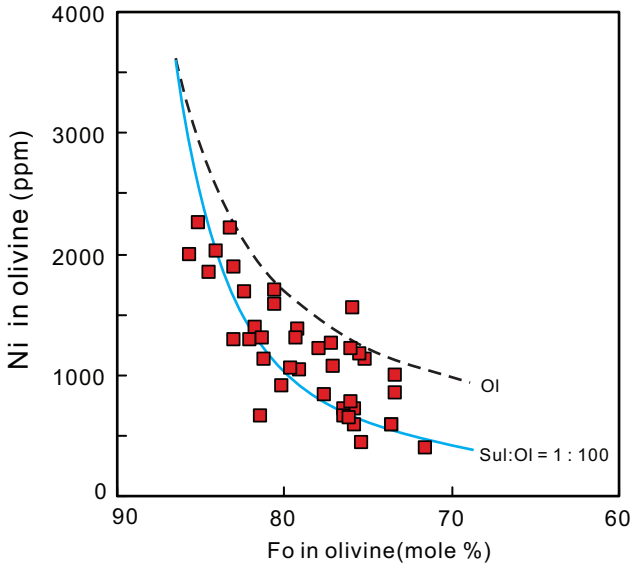

FIG. 16. Fo contents vs. Ni concentrations of the olivine grains in the Piaohechuan no. 4 intrusion.

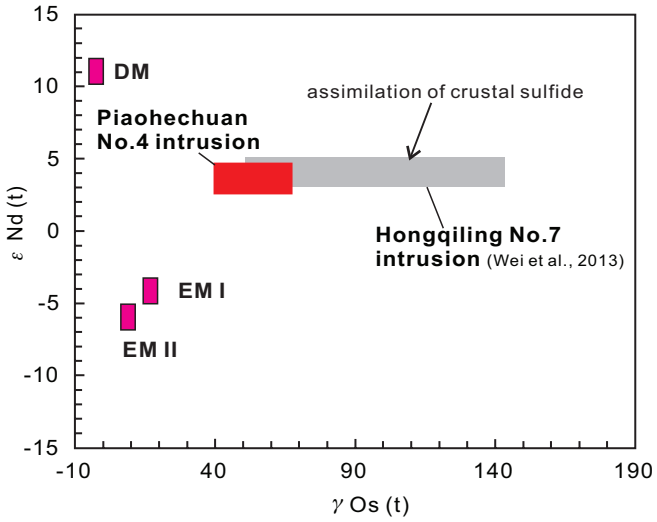

FIG. 17. A plot of $\varepsilon_{Nd(t)}$ vs. $\gamma_{Os(t)}$ values for the rocks in the Piaohechuan no. 4 intrusion. Reservoir end members of the mantle were estimated for Nd (from Zindler and Hart, 1986) and for Os (Shirey and Walker, 1998).

force (Mungall et al., 2015) so that they could be either spherical or irregular (e.g., Fig. 4a). Dowling et al. (2004) proposed that some of the globular disseminated sulfide in the Black Swan deposit in the Yilgarn craton was formed by incorporation of the preexisting, normal interstitial sulfide liquid into the vesicles of silicate rocks during solidification. Recent experimental results indicate that the droplets of sulfide melt can attach to vapor bubbles, forming compound drops that float in silicate melts (Mungall et al., 2015). These compound drops may solidify to globules in the rocks. However, the absence of segregation vesicles near the globular sulfides of the Piaohechuan no. 4 intrusion (Fig. 4a, c, d) indicates that this mechanism did not operate in the Piaohechuan magma chamber.

The sulfides in the different types of the ores in the Piaohechuan no. 4 intrusion are mainly pyrrhotite, and most ores have Ni/Cu ratios ranging from 1.6 to 34 (Fig. 14), indicating that the sulfide liquid is very poor in Cu. The solidus of the Cu-poor sulfide liquid would be close to or higher than 1,000°C (Craig and Kullerud, 1969). On the other hand, abundant primary hornblende in the Piaohechuan no. 4 intrusion (Fig. 3b) indicates that the parental magma was hydrous. A hydrous mafic magma may have a solidus less than 1,000°C (Yoder and Tilley, 1962). In this case, the coalesced sulfide droplets may have been already solidified before the final solidification of silicate melts, forming the globular texture. Such a process was described in the formation of the spherical "buck-shot" ore in the Sudbury Complex (Naldrett, 1969). The interval of the solidus temperature between sulfide droplets and silicate melts resulted in the formation of this special globular texture.

As shown in Figure 4d, the external borders of the globules look as they cut across grains of relatively coarse hornblende or plagioclase, which may be interpreted as the later crystallization of plagioclase and hornblende that impinged along the boundary of the solidified, spherical globule. Silicate crystals that appear in two-dimensional section enclosed in the globules (Fig. 4e) may have crystallized from the silicate melt droplets that penetrate through the sulfide droplets.

Migration of sulfide liquid and origin of the network and breccia ore: In the network ores, bulbous tube-like channels of sulfide formed an interconnected framework through gabbroic rocks (Fig. 5b, c), distinctly different from the commonly recognized net-textured ores; in the breccia ore, the sulfide has aggregated to form a continuous matrix that encloses fragments of gabbro (Fig. 6b). In Figure 6e, a fine-grained fragment with a doleritic texture is located adjacent to several large cumulus-textured crystal fragments, all enclosed in the sulfide matrix. The mosaic of the thin section (PH-3) shows a transition from network ore on the left to breccia ore on the right (Fig. 7), indicating that the two types of sulfide ores formed concurrently and from a similar process.

We propose that sulfide liquid accumulated in the lower part of the intrusion as in other magmatic ore deposits, but following subsequent differentiation and crystallization of the silicate liquid, the sulfide liquid migrated into partially molten silicates along small channels due to overpressure above the silicates. The process by which sulfide liquid could percolate through a crystal mush was considered theoretically by Chung and Mungall (2009) and has been proposed in the Duke Island Complex (Stifter et al., 2014). The migrating sulfide liquid may also have displaced and disaggregated the silicate melt or cumulus crystals into small fragments, forming the net-work and breccia ores of the Piaohechuan no. 4 intrusion. The emulsion texture of the sulfide ores in the Silver San massive sulfide deposit at Black Swan is also attributed to such a process (Dowling et al., 2004).

The distance over which the sulfide migrated remains a matter of speculation. Network textures are present in many samples, but we have observed it only in hand samples or thin sections, and it is probable that this type of sulfide migration occurred only on a small scale. On the other hand, the presence within breccia ores of fragments with contrasting textures, including both cumulate and fine-grained dolerite (Fig. 6e), provides evidence of significant displacement of these fragments after they were incorporated into the

breccia.

Another important feature of these ores is the totally undeformed nature of the host gabbro, lacking tectonic fabrics. The rock is commonly altered, but during the transition to secondary assemblages, the rock largely retained its primary magmatic texture. We therefore conclude that the breccia is not tectonic. The transition from network to breccia ore indicates that the breccia formed when the proportion of sulfide exceeded a certain limit—around 50% judging from sample PH-3 and other samples (see Fig 7). In sulfide-rich samples, the fabric of the rock breaks down and fragments of gabbro are entrained into a sulfide matrix. In intrusions with the dimensions of the Piaohechuan no. 4 intrusion, cumulus rocks normally are limited to interior portions, tens of meters from chilled margins. The coexistence of cumulus and fine-grained samples in the breccia therefore indicates the displacement of sulfide at this scale. If this is indeed the case, then the migration of sulfide liquid may play an important role in the distribution of the ore and therefore in the formation of the ore deposit.

Redistribution of sulfide and secondary silicate minerals during metamorphism: In Figure 4d and f, tremolite crystals are growing into the sulfide bleb. The secondary minerals in altered rocks are tremolite, talc, and chlorite (Figs. 3a, 4f, 6e), an assemblage that forms at low temperatures around 300° to 500°C, well below the sulfide solidus (~1,000°C, Naldrett, 1969). It appears that the silicate rocks were altered after the sulfide textures had formed, resulting in irregular contacts between sulfide and secondary silicate minerals (Figs. 5f, 6f). In most of the sulfide ores, the silicate portions were totally altered, but some fragments of silicate rocks and crystals in breccia ores are relatively fresh (Fig. 6c, d). It seems that the sulfides formed a protective jacket around the silicate phases and prevented the fluids from penetrating during metamorphism. Minor redistribution of sulfide and secondary silicate minerals probably continued during metamorphism after the major magmatic textures had formed.

Conclusions

The parental magma of the Piaohechuan no. 4 intrusion was high Mg basaltic and PGE depleted. Sulfide saturation of the parental magma was triggered by olivine crystallization and the addition of external crustal sulfide in a shallow chamber. The globular ores formed when the coalesced sulfide droplets were largely solid before the final solidification of silicate minerals. The textures of network and breccia ores were produced when sulfide liquid invaded partially molten silicates, displacing and disaggregating the silicate melt or cumulus crystals into small fragments. Migration of sulfide liquid may influence the present distribution of the ores in the intrusion.

Acknowledgments

This study was supported by NSFC grants 41325006, 41403037, and 41421062, and GIGCAS 135 project Y234041001. Arndt thanks China Ministry of Education, Oversea Outstanding Professors project MS2011ZGDZ[BJ]019 for support. Aihua Xi of Jilin University and Tianxi Gu and Yanmei Liu of the Jinlin Nickel Company are thanked for field assistance. We thank two reviewers and associate editor, Steve Barnes, for their constructive comments which significantly improved the paper. This is contribution IS-2084 from Guangzhou Institute of Geochemistry, Chinese Academy of Sciences.

REFERENCES

Arndt, N.T., 2011, Insights into the geologic setting and origin of Ni-Cu-PGE sulfide deposits of the Norilsk-Talnakh region, Siberia: Reviews in Economic Geology, v. 17, p. 199–215.

Arndt, N.T., Czamanske, G.K., Walker, R.J, Chauvel, C., and Fedorenko, V.A., 2003, Geochemistry and origin of the intrusive hosts of the Noril'sk-Talnakh Cu-Ni-PGE sulfide deposits: Economic Geology, v. 98, p. 495–515.

Barnes, S.J., 2006, Komatiite-hosted nickel sulfide deposits of the Yilgarn craton: Geology, Geochemistry, and Genesis, 210 p.

Barnes, S.J., and Lightfoot, P.C., 2005, Formation of magmatic nickel sulfide ore deposits and processes affecting the Cu and PGE contents: Economic Geology 100th Anniversary Volume, p. 179–214.

Barnes, S.J., and Maier, W., 1999, The fractionation of Ni, Cu and the noble metals in silicate and sulphide liquids: Dynamic processes in magmatic ore deposits and their application to mineral exploration: Geological Association of Canada, Short Course Notes, v. 13, p. 69–106.

Barnes, S.J., Gole, M.J., and Hill, R.E.T., 1988, The Agnew nickel deposit, Western Australia. Part I. Structure and stratigraphy: Economic Geology, v. 83, p. 524–536.

Barnes, S.J., Wells, M.A., and Verrall, M.R., 2009, Effects of magmatic processes, serpentinization, and talc-carbonate alteration on sulfide mineralogy and ore textures in the Black Swan disseminated nickel sulfide deposit, Yilgarn craton: Economic Geology, v. 104, p. 539–562.

Birck, J.L., Barman, M.R., and Capmas, F., 1997, Re-Os isotopic measurements at the femto mole level in natural samples: Geostandards Newsletter, v. 21, p. 19–27.

Chai, S.L., Ren, H.M., Shen, Q.G., and Wang, D.Y., 2003, Geological and geochemical comparison between Ni-mineralization and Ni-nonmineralization intrusions in Hongqiling area of Jilin Province: Contributions to Geology and Mineral Resources Research, v. 18, p. 229–232 (in Chinese with English abs.).

Chung, H.Y., and Mungall, J.E., 2009, Physical constraints on the migration of immiscible fluids through partially molten silicates, with special reference to magmatic sulfide ores: Earth and Planetary Science Letters, v. 286, p. 14–22.

Craig, J.R., and Kullerud, G., 1969, Phase relations in the Cu-Fe-Ni-S system and their application to magmatic ore deposits: Economic Geology Monograph 4, p. 344–358.

Dare, S.A.S., Barnes, S-J., Prichard, H.M., and Fisher, P.C., 2010, The timing and formation of platinum-group minerals from the Creighton Ni-Cu-platinum group element sulfide deposit, Sudbury, Canada: Early crystallization of PGE-rich sulfarsenides: Economic Geology, v. 105, p. 1071–1096.

De Bremond D'ars, J., Arndt, N.T., and Hallot, E., 2001, Analog experimental insights into the formation of magmatic sulfide deposits: Earth and Planetary Science Letters, v. 186, p. 371–381.

Dowling, S.E., Barnes, S.J., Hill, R.E.T., and Hicks, J.D., 2004, Komatiites and nickel sulfide ores of the Black Swan area, Yilgarn craton, Western Australia. 2: Geology and genesis of the orebodies: Mineralium Deposita, v. 39, p. 707–728.

Fleet, M.E., Chryssoulis, S.L., Stone, W.E., and Weisener, C.G., 1993, Partitioning of platinum-group elements and Au in the Fe-Ni-Cu-S system: Experiments on the fractional crystallization of sulfide melt: Contributions to Mineralogy and Petrology, v. 115, p. 36–44.

Francis, R.D., 1990, Sulfide globules in mid-ocean ridge basalts (MORB), and the effect of oxygen abundance in Fe-S-O liquids on the ability of those liquids to partition metals from MORB and komatiite magmas: Chemical Geology, v. 85, p. 199–213.

Godel, B., 2013, High-resolution X-ray computed tomography and its application to ore deposits: From data acquisition to quantitative three-dimensional measurements with case studies from Ni-Cu-PGE deposits: Economic Geology, v. 108, p. 2005–2019.

Godel, B., González-Ivarez, I., Barnes, S.J., Barnes, S-J., Parker, P., and Day, J., 2012, Sulfides and sulfarsenides from the Rosie nickel prospect, Duketon greenstone belt, Western Australia: Economic Geology, v. 107, p. 275–294.

Hanley, J.J., 2007, The role of arsenic-rich melts and mineral phases in the

development of high-grade Pt-Pd mineralization within komatiite-associated magmatic Ni-Cu sulfide horizons at Dundonald Beach South, Abitibi subprovince, Ontario, Canada: Economic Geology, v. 102, p. 305–317.
Hao, L.B., Sun, L.J., Zhao, Y.Y., and Lu, J.L., 2013, SHRIMP zircon U-Pb dating of Chajian mafic-ultramafic rocks in Hongqiling mine field, Jilin province, and its implications: Earth Science-Journal of China University of Geosciences, p. 233–240 (in Chinese with English abs.).
Hem, S.R., and Makovicky, E., 2004, The system Fe-Co-Ni-As-S. 1. Phase relations in the (Fe, Co, Ni)$As_{0.5}S_{1.5}$ section at 650° and 500°C: Canadian Mineralogist, v. 42, p. 43–62.
Holwell, D.A., Abraham-James, T., Keays, R.R., and Boyce, A.J., 2012, The nature and genesis of marginal Cu-PGE-Au sulphide mineralisation in Paleogene macrodikes of the Kangerlussuaq region, East Greenland: Mineralium Deposita, v. 47, p. 3–21.
Holzheid, A., 2010, Separation of sulfide melt droplets in sulfur saturated silicate liquids: Chemical Geology, v. 274, p. 127–135.
Jilin Bureau of Geology and Mineral Resources (JBGMR), 1980, Geological survey of the Piaohechuan no. 4 and no. 5 intrusions in Jiaohe country, Jinlin province: Unpublished report, p. 1–83 (in Chinese).
Jochum, K., Arndt, N., and Hofmann, A., 1991, Nb-Th-La in komatiites and basalts: Constraints on komatiite petrogenesis and mantle evolution: Earth and Planetary Science Letters, v. 107, p. 272–289.
Klemm, D.D., 1965, Synthesen und Analysen in den Dreiecksdiagrammen FeAsS-CoAsS-NiAsS und FeS_2-CoS_2-NiS_2: Neus Jahrbuch fuer Mineralogie Abhandlungen, v. 103, p. 205–255.
Lambert, D.D., Frick, L.R., Foster, J.G., Li, C., and Naldrett, A.J., 2000, Re-Os isotope systematics of the Voisey's Bay Ni-Cu-Co magmatic sulfide system, Labrador, Canada: II. Implications for parental magma chemistry, ore genesis, and metal redistribution: Economic Geology, v. 95, p. 867–888.
Lesher, C.M., 1983, Localization and genesis of komatiite-associated Fe-Ni-Cu sulphide mineralization at Kambalda, Western Australia: Unpublished Ph.D. thesis, University of Western Australia, 318 p.
——2007, Ni-Cu-(PGE) deposits in the Raglan area, Cape Smith belt, New Québec: Mineral deposits of Canada: A synthesis of major deposit-types, district metallogeny, the evolution of geological provinces, and exploration methods: Geological Association of Canada, Mineral Deposits Division, Special Publication, v. 5, p. 351–386.
Li, C.F., Li, X.H., Li, Q.L., Guo, J.H., and Liu, T., 2011, An evaluation of a single-step extraction chromatography separation method for Sm-Nd isotope analysis of micro-samples of silicate rocks by high-sensitivity thermal ionization mass spectrometry: Analytica Chimica Acta, v. 706, p. 297–304.
Li, C.S., Maier, W.D., and De Waal, S., 2001, Magmatic Ni-Cu versus PGE deposits: Contrasting genetic controls and exploration implications: South African Journal of Geology, v. 104, p. 309–318.
Li, C.S., Ripley, E.M., And Naldrett, A.J., 2003, compositional variations of olivine and sulfur isotopes in the Noril'sk and Talnakh intrusions, Siberia: Implications for ore-forming processes in dynamic magma conduits: Economic Geology, v. 98, p. 69–86.
Li, C.S., Zhang, M., Fu, P., Qian, Z., Hu, P., and Ripley, E., 2012, The Kalatongke magmatic Ni-Cu deposits in the Central Asian orogenic belt, NW China: Product of slab window magmatism?: Mineralium Deposita, v. 47, p. 51–67.
Lü, L.S., Mao, J.W., Liu, J., Zhang, Z.H., and Xie, G.Q., 2007, Geochronology and tectonic settings of typical magmatic Ni-Cu-(PGE) sulfide deposits in the northern margin of the North China craton: Acta Geoscientica Sinica, v. 2, p. 148–166 (in Chinese with English abstract).
Lü, L.S., Mao, J.W., Li, H.B., Pirajno, F., Zhang, Z.H., and Zhou, Z.H., 2011, Pyrrhotite Re-Os and SHRIMP zircon U-Pb dating of the Hongqiling Ni-Cu sulfide deposits in Northeast China: Ore Geology Reviews, v. 43, p. 106–119.
McInnes, B.I., Mcbride, J.S., Evans, N.J., Lambert, D.D., and Andrew, A.S., 1999, Osmium isotope constraints on ore metal recycling in subduction zones: Science, v. 286, p. 512–516.
Mungall, J.E., Brenan, J.M., Godel, B., Barnes, S.J., and Gaillard, F., 2015, Transport of metals and sulphur in magmas by flotation of sulphide melt on vapour bubbles: Nature Geoscience, v. 8, p. 216–219.
Naldrett, A.J., 1969, A portion of the system Fe-S-O between 900° and 1080°C and its application to sulfide ore magmas: Journal of Petrology, v. 10, p. 171–201.
——2010, Secular variation of magmatic sulfide deposits and their source magmas: Economic Geology, v. 105, p. 669–688.
Naldrett, A.J., and Duke, J.M., 1980, Platinum metals in magmatic sulfide ores: Science, v. 208, p. 1417–1424.
Naldrett, A.J., Lightfoot, P.C., Fedorenko, V., Doherty, W., and Gorbachev, N.S., 1992, Geology and geochemistry of intrusions and flood basalts of the Noril'sk region, USSR, with implications for the origin of the Ni-Cu ores: Economic Geology, v. 87, p. 975–1004.
O'Hara, M., 1968, The bearing of phase equilibria studies in synthetic and natural systems on the origin and evolution of basic and ultrabasic rocks: Earth-Science Reviews, v. 4, p. 69–133.
Pattison, E.F., 1979, The Sudbury sublayer: Canadian Mineralogist, v. 17, p. 257–274.
Prichard, H.M., Hutchinson, D., and Fisher, P.C., 2004, Petrology and crystallization history of multiphase sulfide droplets in a mafic dike from Uruguay: Implications for the origin of Cu-Ni-PGE sulfide deposits: Economic Geology, v. 99, p. 365–376.
Prichard, H.M., Fisher, P.C., Mcdonald, I., Knight, R.D., Sharp, D.R., and Williams, J.P., 2013, The distribution of PGE and the role of arsenic as a collector of PGE in the Spotted Quoll nickel ore deposit in the Forrestania greenstone belt, Western Australia: Economic Geology, v. 108, p. 1903–1921.
Ripley, E.M., Park, Y.R., Li, C., and Naldrett, A.J., 1999, Sulfur and oxygen isotopic evidence of country rock contamination in the Voisey's Bay Ni-Cu-Co deposit, Labrador, Canada: Lithos, v. 47, p. 53–68.
Roeder, P.L., and Emslie, R.F., 1970, Olivine-liquid equilibrium: Contributions to Mineralogy and Petrology, v. 29, p. 275–289.
Rudnick, R., and Gao, S., 2003, Composition of the continental crust: Treatise on Geochemistry, v. 3, p. 1–64.
Saunders, A., Norry, M., and Tarney, J., 1991, Fluid influence on the trace element compositions of subduction zone magmas: Philosophical Transactions of the Royal Society of London. Series A: Physical and Engineering Sciences, v. 335, p. 377–392.
Shirey, S.B., and Walker, R.J., 1995, Carius tube digestion for low-blank rhenium-osmium analysis: Analytical Chemistry, v. 67, p. 2136–2141.
——1998, The Re-Os isotope system in cosmochemistry and high-temperature geochemistry: Annual Review of Earth and Planetary Sciences, v. 26, p. 423–500.
Stifter, E.C., Ripley, E.M., and Li, C.S., 2014, Silicate melt removal and sulfide liquid retention in ultramaficrocks of the Duke Island Complex, southeastern Alaska: Mineralogy and Petrology, v. 108, p. 727–740.
Sun, S.S., and Mcdonough, W.F., 1989, Chemical and isotopic systematics of oceanic basalts: Implications for mantle composition and processes: Geological Society, London, Special Publication 42, p. 313–345.
Sun, Y.L., Chu, Z.Y., Sun, M., and Xia, X.P., 2009, An improved Fe-Ni sulfide fire assay method for determination of Re, platinum group elements, and Os isotopic ratios by inductively coupled plasma-and negative thermal ionization-mass spectrometry: Applied Spectroscopy, v. 63, p. 1232–1237.
Thakurta, J., Ripley, E.M., and Li, C., 2008, Geochemical constraints on the origin of sulfide mineralization in the Duke Island Complex, southeastern Alaska: Geochemistry, Geophysics, Geosystems, v. 9, p. 1–34.
Vroon, P., Bergen, M.V., White, W., and Varekamp, J., 1993, Sr-Nd-Pb isotope systematics of the Banda arc, Indonesia: Combined subduction and assimilation of continental material: Journal of Geophysical Research: Solid Earth (1978–2012), v. 98, p. 22,349–22,366.
Walker, R.J., Carlson, R.W., and Shirey, S.B., 1989, Os, Sr, Nd, and Pb isotope systematics of southern African peridotite xenoliths: Implications for the chemical evolution of subcontinental mantle: Geochimica et Cosmochimica Acta, v. 53, p. 1583–1595.
Wang, C.Y., Zhou, M.F., and Qi, L., 2007, Permian flood basalts and mafic intrusions in the Jinping (SW China)-Song Da (northern Vietnam) district: Mantle sources, crustal contamination and sulfide segregation: Chemical Geology, v. 243, p. 317–343.
Wei, B., Wang, C.Y., Li, C.S., and Sun, Y.L., 2013, Origin of PGE-depleted Ni-Cu sulfide mineralization in the Triassic Hongqiling no. 7 orthopyroxenite intrusion, Central Asian orogenic belt, northeastern China: Economic Geology, v. 108, p. 1813–1831.
Windley, B.F., Alexeiev, D., Xiao, W., Kröner, A., and Badarch, G., 2007, Tectonic models for accretion of the Central Asian orogenic belt: Journal of the Geological Society, v. 164, p. 31–47.
Wood, M., 2003, Arsenic in igneous systems: An experimental investigation: B.A.Sc. thesis, Toronto, Ontario, Canada, University of Toronto, 32 p.
Wu, F.Y., Wilde, S.A., Zhang, G.L., and Sun, D.Y., 2004, Geochronology and petrogenesis of the post-orogenic Cu-Ni sulfide-bearing mafic-ultramafic complexes in Jilin province, NE China: Journal of Asian Earth Sciences,

v. 23, p. 781–797.
Wu, F.Y., Zhao, G.C., Sun, D.Y., Wilde, S.A., and Yang, J.H., 2007, The Hulan Group: Its role in the evolution of the Central Asian orogenic belt of NE China: Journal of Asian Earth Sciences, v. 30, p. 542–556.
Wu, F.Y., Sun, D.Y., Ge, W.C., Zhang, Y.B., Grant, M.L., Wilde, S.A., and Jahn, B.M., 2011, Geochronology of the Phanerozoic granitoids in northeastern China: Journal of Asian Earth Sciences, v. 41, p. 1–30.
Xiao, W.J., Windley, B.F., Yong, Y., Yan, Z., Yuan, C., Liu, C., and Li, J., 2009, Early Paleozoic to Devonian multiple-accretionary model for the Qilian Shan, NW China: Journal of Asian Earth Sciences, v. 35, p. 323–333.
Xie, H.Q., Zhang, F.Q., Miao, L.C., Li, T.S., and Liu, D.Y., 2007, Characteristics of the Piaohechuan mafic-ultramafic complex, central Jilin, northeast China: Constrains on the nature and evolution of the northeastern North China marginal tectonic belt: Geological Bulletin of China, v. 26, p. 810–822.
Yang, S.H., Zhou, M.F., Lightfoot P.C., Malpas J., Qu, W.J., Zhou, J.B., and Kong D.Y., 2012, Selective crustal contamination and decoupling of lithophile and chalcophile element isotopes in sulfide-bearing mafic intrusions: An example from the Jingbulake intrusion, Xinjiang, NW China: Chemical Geology v. 302–303, p. 106–118.
Yang, Y.H., Zhang, H.F., Chu, Z.Y., Xie, L.W., and Wu, F.Y., 2010, Combined chemical separation of Lu, Hf, Rb, Sr, Sm and Nd from a single rock digest and precise and accurate isotope determinations of Lu-Hf, Rb-Sr and Sm-Nd isotope systems using multi-collector ICP-MS and TIMS: International Journal of Mass Spectrometry, v. 290, p. 120–126.
Yoder, H.S., and Tilley, C.E., 1962, Origin of basalt: An experimental study of nature and synthetic rock systerm: Journal of Petrology, v. 3, p. 342–532.
Zindler, A., and Hart, S., 1986, Chemical geodynamics: Annual Review of Earth and Planetary Sciences, v. 14, p. 493–571.

Analytical Methods

APPENDIX

Whole-rock major oxides and S contents

Whole-rock major element compositions and S were analyzed at the National Research Center for Geoanalysis (NRCG), China. For analysis of the major elements portions of powdered samples (30 mg) were mixed with lithium metaborate (130 mg) and then fused at 1,000°C for 15 min. The liquid melts were poured into glass beakers containing 15 ml 5% aqua regia and the beakers were placed in an ultrasonic machine. After ultrasonic dissolution for 15 min, the melts were dissolved and then made up to 25 ml with 5% aqua regia for determination of major elements by ICP-AES. During sample preparation, Chinese certified reference materials (CRM), GSR-3, GSR-9, and GSR-11, and two sample blanks were analyzed in every batch. These CRM solutions were employed for standardization of the ICP-AES (IRIS-Advantage, ThermoFisher Scientific, United States). During the ICP-AES measurements, the CRM solutions were run every 10 samples in order to monitor the instrumental drift. Cd as an internal standard was employed and its concentration in each sample solution is 1 μg/ml. Using this method, the analytical precision is better than 1.5%.

For analysis of S content, the conventional $BaSO_4$ gravimetric method was used. A weight of 0.25 g of each sample was mixed with 3.5 g of flux composed of Na_2CO_3 and ZnO (Na_2CO_3:ZnO = 3:2) which were sintered at 800°C. Then the samples were leached and supernatants were collected. Using a methyl orange solution as an indicator, the supernatants were neutralized by 50% HCl. When the solutions became red, an excess of 3 ml 50% HCl was added. With addition of water, the sample solutions were made up to ~300 ml and then heated to boiling. During stirring 15 ml of 100 mg/ml $BaCl_2$ solution was added and $BaSO_4$ precipitates were formed. These samples were heated to boiling and then warmed until the upper liquid became clear. After aging for 4 h, the $BaSO_4$ precipitates were collected and washed until no Cl ions remained. The precipitates were ashed at 800°C until their weights became constant. Using the weight of $BaSO_4$ precipitates, the S content of samples was calculated. Whole-rock major element compositions and S were obtained using a gravimetric method at the National Research Center for Geoanalysis, China.

Mineral composition

PGM mineralogical studies were performed on eight thin sections of samples from the Piaohechuan no. 4 intrusion. Petrography was examined using conventional optical microcopy, and minerals were analyzed using a Cambridge Instruments S360 scanning electron microscope (SEM) in the Cardiff University. Polished sections were searched for PGM systematically using the SEM set at magnification of ×100. Quantitative analyses of the larger PGM were obtained using an Oxford Instruments INCA Energy EDX analyzer attached to the SEM. Operating conditions for the quantitative analyses were 20 kV, with specimen calibration current of ~1 nA and a working distance of 25 mm. A cobalt reference standard was regularly and frequently analyzed, in order to check for any drift in the analytical condition. A comprehensive set of standards obtained from MicroAnalysis Consultants Ltd. (St Ives, Cambridgeshire) was used to calibrate the EDX analyzer. Images were obtained using a four-quadrant backscattered detector operating at 20 kV, a beam current of ~500 pA, and a working distance of 13 mm, under which conditions magnifications up to x15000 are possible. To place the PGM in context mineralogically, the associated silicate and sulfide minerals were identified using the SEM.

Olivine compositions were analyzed by a JEOL JXA-8100 electron microprobe at the Guangzhou Institute of Geochemistry, Chinese Academy of Sciences. The standards used were olivine for Si, Mg, Fe, and Ni, rutile for Ti, garnet for Al and Ca, feldspar for Na, MnO for Mn, and Cr_2O_3 for Cr. The precision of analyses is better than 2% for SiO_2, FeO, and MgO, and better than 5% for other components. The experimental

conditions used a focused beam in spot mode with a beam diameter of 1 to 2 mm, accelerating voltage at 15 kV and beam current at 20 nA. Peak counting time was set at 30 s for Ca and Ni, 7 s for Na, 8 s for K, and 10 s for other elements. Background counting time was set at 15 s. The raw data were calibrated using the ZAF method.

Whole-rock platinum-group elements

Platinum-group elements were analyzed by an improved Fe-Ni sulfide fire assay method at the Guangzhou Institute of Geochemistry, CAS. Each of the samples was mixed with 40 g $Na_2B_4O_7$, 2.5 g Fe, 1 g Ni, and 1 g S, and transferred to a fired-clay crucible at 1,050°C for 45 min. After cooling, the resulting sulfide bead was placed in a glass beaker containing 15 ml H_2O. The bead was disintegrated into powder, and then 30 ml of HCl was added. Upon heating, the solution became clear and was then filtered to collect any insoluble residue. This residue was transferred into distillation apparatus with 3 ml HNO_3 and Os was distilled at 110°C for 30 min as OsO_4, which was absorbed with 5 ml H_2O for ICP-MS determination of the Os content. The remaining solution was concentrated to about 1 ml and then 2 ml of HCl was added to ensure dissolution of the PGE residue. The solution was evaporated to a small volume, then 1 ml of concentrated HNO_3 was added and the solution heated for effective removal of Os as volatile OsO_4. Finally, the small remaining solution was made up to 10 ml H_2O for analysis of Ru, Rh, Ir, Pd, and Pt by ICP-MS (Perkin-Elmer Sciex Elan6000). A detailed account of this method for PGE analysis is presented by Sun et al. (2009).

Whole-rock Sr-Nd isotope composition

Whole-rock Sr-Nd isotope data were obtained at the Institute of Geology and Geophysics, CAS. Powders for Sr and Nd isotope analyses were dissolved in a Savillex Teflon screw-top capsule after being spiked with mixed ^{87}Rb-^{84}Sr and ^{149}Sm-^{150}Nd tracers prior to HF + HNO_3 + $HClO_4$ dissolution. Rb, Sr, Sm, and Nd were separated using the classical two-step ion exchange chromatographic method and measured using a Finnigan MAT262 multicollector thermal ionization mass spectrometer. The Rb-Sr and Sm-Nd isotope analysis followed procedures similar to those described by Yang et al. (2010). During the whole procedure the blank was lower than 300 pg for Rb-Sr and 100 pg for Sm-Nd. The isotopic ratios were corrected for mass fractionation by normalizing to $^{88}Sr/^{86}Sr$ = 8.375209 and $^{146}Nd/^{144}Nd$ = 0.7219, respectively. The international standard samples, NBS-987 and JNdi-1, were employed to evaluate instrument stability during the period of data collection. The measured values for the NBS-987 Sr standard and JNdi-1 Nd standard were $^{87}Sr/^{86}Sr$ = 0.710242 ± 0.000010 (n = 8, 2σ) and $^{143}Nd/^{144}Nd$ = 0.512111 ± 0.000013 (n = 8, 2σ), respectively. USGS reference material BCR-2 was measured to monitor the accuracy of the analytical procedures, with the following results: $^{87}Sr/^{86}Sr$ = 0.705011 ± 0.000013 and $^{143}Nd/^{144}Nd$ = 0.512634 ± 0.000014. The $^{87}Sr/^{86}Sr$ and $^{143}Nd/^{144}Nd$ data of BCR-2 show good agreement with previously published data by TIMS and MC-ICP-MS techniques (Yang et al., 2010; Li et al., 2011).

Whole-rock Re-Os isotope composition

Whole-rock Os isotope compositions and Os concentrations were analyzed by a Triton negative thermal ionization mass spectrometer (NTIMS) at Guangzhou Institute of Geochemistry, CAS. Re concentrations of the rocks of the intrusion were determined using an X Series-2 quadrupole ICP-MS at Guangzhou Institute of Geochemistry. Samples (1–4 g) were digested in Carius tubes using aqua regia following the method of Shirey and Walker (1995). After digestion, Os and Re were purified following the method of Birck et al. (1997). Os isotope fractionation was corrected for using $^{188}Os/^{192}Os$ = 0.32440. During the period of analysis, analyses of WPR-1 standard yielded an average $^{187}Os/^{188}Os$ ratio of 0.14521 ± 28 (2σ).